Principal Oscillation Patterns: A Review

HANS VON STORCH, GERD BÜRGER, REINER SCHNUR, AND JIN-SONG VON STORCH

Max-Planck-Institut für Meteorologie, Hamburg, Germany

(Manuscript received 13 October 1993, in final form 23 May 1994)

ABSTRACT

The *principal oscillation pattern* (POP) analysis is a technique used to simultaneously infer the characteristic patterns and timescales of a vector time series. The POPs may be seen as the normal modes of a linearized system whose system matrix is estimated from data.

The concept of POP analysis is reviewed. Examples are used to illustrate the potential of the POP technique. The best defined POPs of tropospheric day-to-day variability coincide with the most unstable modes derived from linearized theory. POPs can be derived even from a space–time subset of data. POPs are successful in identifying two independent modes with similar timescales in the same dataset.

The POP method can also produce forecasts that may potentially be used as a reference for other forecast models.

The conventional POP analysis technique has been generalized in various ways. In the *cyclostationary* POP analysis, the estimated system matrix is allowed to vary deterministically with an externally forced cycle. In the *complex* POP analysis, not only the state of the system but also its "momentum" is modeled.

Associated correlation patterns are a useful tool to describe the appearance of a signal previously identified by a POP analysis in other parameters.

1. Introduction

The POP (*principal oscillation pattern*) analysis is a multivariate technique to empirically infer the characteristics of the space–time variations of a possibly complex system (Hasselmann 1988; von Storch et al. 1988). The basic idea is to identify a linear system with a few free parameters that are fitted to the data. Then, the space–time characteristics of this simple system is regarded as being the same as those of the full system. In the present paper we review the state of the art of POP analysis including two recent offsprings, the *cyclostationary* POP analysis (Blumenthal 1991) and the *complex* POP analysis (Bürger 1993).

The POP analysis is nowadays a routinely used tool (Gallagher et al. 1991) to diagnose the space–time variability of the climate system. Processes analyzed with POPs are

- the Madden and Julian oscillation, also named the tropical 30–60 day oscillation (von Storch et al. 1988; von Storch and Xu 1990; von Storch and Baumhefner 1991; von Storch and Smallegange 1991),
- oceanic variability (Mikolajewicz 1990; Weisse et al. 1994),
- the stratospheric quasi-biennial oscillation (Xu 1992),
- the El Niño/Southern Oscillation (ENSO) (Xu and von Storch 1990; Xu 1990; Latif et al. 1993; Blumenthal 1991; Latif and Villwock 1989; Latif and Flügel 1990; Bürger 1993; Xu 1992; Penland and Magorian 1993; Xue et al. 1994; Wu et al. 1994; Tang 1994; Tang et al. 1994),
- tropospheric baroclinic waves (Schnur et al. 1993; Schnur 1993),
- low-frequency variability in the coupled atmosphere–ocean system (Xu 1993; von Storch 1994), and
- Arctic variability (Tang et al. 1994).

In section 2 of this paper, the POPs are introduced in two conceptually different ways. One way is to define POPs as normal modes of a linear system, the parameters of which are inferred from a vector time series. The other way is to regard POPs as a simplified and special version of Principal Interaction Patterns (PIPs). The PIP formulation (Hasselmann 1988) is a fairly general approach that allows for a large variety of complex scenarios. In section 3, three examples of a POP analysis are given. One example, on tropospheric baroclinic waves (Schnur 1993), is to demonstrate the normal mode concept of the POPs. The best defined POPs coincide, to good approximation, with the most unstable modes derived in a conventional stability analysis of the linearized dynamical equations. The other two examples have been chosen to show the ability of the POP analysis to detect signals in different situations. In the joint POP analysis of tropospheric and stratospheric data (Xu 1992) two independent

Corresponding author address: Dr. Hans von Storch, Max-Planck-Institut für Meteorologie, Bundesstrasse 55, Hamburg D-20146, Germany.

modes with similar timescales, the Southern Oscillation (SO) and the quasi-biennial oscillation (QBO), are identified. In the POP analysis of the Madden and Julian oscillation (MJO) (von Storch and Xu 1990), the signal has a well-defined signature all along the equator, but it is possible to identify the signal already in 90° subsectors. Also, the signal is the same whether the analysis is based on two years of data or on five years of data.

Since a POP analysis implies the fit of a time series model to data, the POP approach incorporates a predictive potential (section 4). As an example, the skill in predicting the state of the MJO is shown and compared to the skill of a numerical weather prediction model.

In sections 5 and 6, two generalizations of the POP analysis are presented: the cyclostationary POP analysis and the complex POP analysis. In section 7 the concept of associated correlation patterns is introduced, and the paper is concluded in section 8 with some remarks on the general merits and limitations of the POP technique.

2. Principal oscillation patterns

The following notations are used: vectors are given as bold letters and matrices as calligraphic letters, such as $\mathcal{A}$ or $\mathcal{X}$. If $\mathcal{A}$ is a matrix, then $\mathcal{A}^T$ is the transposed matrix. If x is any complex quantity, then x^* is its conjugate complex.

It should be noted that the POP formalism—conventional, cyclostationary, and complex POP analysis—may be applied to linear systems whose system matrices are estimated from data or whose system matrices are derived from theoretical dynamical considerations (see also section 3a).

a. *POPs and normal modes*

The normal modes of a linear discretized real system,

$$\mathbf{x}(t+1) = \mathcal{A}\cdot\mathbf{x}(t), \tag{1}$$

are the eigenvectors $\mathbf{p}$ of the matrix $\mathcal{A}$. In general, $\mathcal{A}$ is not symmetric and some or all of its eigenvalues λ and eigenvectors $\mathbf{p}$ are complex. However, since $\mathcal{A}$ is a real matrix, the conjugate complex quantities λ^* and $\mathbf{p}^*$ satisfy also the eigenequation $\mathcal{A}\cdot\mathbf{p}^* = \lambda^*\mathbf{p}^*$. In most cases, all eigenvalues are different and the eigenvectors form a linear basis. So, the state $\mathbf{x}$ at any time t may be uniquely expressed in terms of the eigenvectors:

$$\mathbf{x} = \sum_j z_j\cdot\mathbf{p}_j. \tag{2}$$

The coefficients of the pairs of conjugate complex eigenvectors are conjugate complex too. Inserting (2) into (1) we find that the coupled system (1) becomes uncoupled, yielding n single equations, where n is the dimension of the process $\mathbf{x}$,

$$z(t+1)\cdot\mathbf{p} = \lambda\cdot z(t)\cdot\mathbf{p} \tag{3}$$

so that, if $z(0) = 1$,

$$z(t)\cdot\mathbf{p} = \lambda^t\cdot\mathbf{p} \tag{4}$$

(dropping indices). The contribution $\mathbf{P}(t)$ of the complex conjugate pair $\mathbf{p}$, $\mathbf{p}^*$ to the process $\mathbf{x}(t)$ is given by

$$\mathbf{P}(t) = z(t)\cdot\mathbf{p} + [z(t)\cdot\mathbf{p}]^*. \tag{5}$$

Writing $\mathbf{p} = \mathbf{p}^r + i\cdot\mathbf{p}^i$ and $2z(t) = z^r(t) - i\cdot z^i(t)$, this reads

$$\begin{aligned}\mathbf{P}(t) &= z^r(t)\cdot\mathbf{p}^r + z^i(t)\cdot\mathbf{p}^i \\ &= \rho^t(\cos(\eta t)\cdot\mathbf{p}^r - \sin(\eta t)\cdot\mathbf{p}^i)\end{aligned} \tag{6}$$

with $\lambda = \rho\exp(-i\eta)$ and $z(0) = 1$. The geometric and physical meaning of (6) is the trajectory spirals in the space spanned by $\mathbf{p}^r$ and $\mathbf{p}^i$ (Fig. 1) with the *period* $T = 2\pi/\eta$ and the *e-folding time* $\tau = -1/\ln(\rho)$ in the consecutive order

$$\cdots\rightarrow\mathbf{p}^r\rightarrow-\mathbf{p}^i\rightarrow-\mathbf{p}^r\rightarrow\mathbf{p}^i\rightarrow\mathbf{p}^r\rightarrow\cdots. \tag{7}$$

The e-folding time τ is the time needed to reduce an initial amplitude $|z(0)| = 1$ to $|z(\tau)| = 1/e$. We will label this time as *the damping time.* The period is the time needed to fulfill one complete cycle in (7).

Any eigenvector $\mathbf{p}$ is determined up to a complex scalar α. To make things unique, one can choose α in such a way that $\mathbf{p}^r$ and $\mathbf{p}^i$ are orthogonal and $|\mathbf{p}^r| \geqslant |\mathbf{p}^i|$.

The modes may be represented either by the two patterns $\mathbf{p}^r$ and $\mathbf{p}^i$ or by plots of the local wave amplitude $A^2(\mathbf{r}) = [\mathbf{p}^r(\mathbf{r})]^2 + [\mathbf{p}^i(\mathbf{r})]^2$ and relative phase $\psi(\mathbf{r}) = \tan^{-1}[\mathbf{p}^i(\mathbf{r})/\mathbf{p}^r(\mathbf{r})]$ (Fig. 2). The transformation in (7) between the patterns $\mathbf{p}^r$ and $\mathbf{p}^i$ can assume various geometric wave forms. If $\mathbf{p}^i(\mathbf{r}) = \mathbf{p}^r(\mathbf{r} - \mathbf{r}_0)$, with a location vector $\mathbf{r}$ and a fixed vector $\mathbf{r}_0$, the signal appears as a parallel crested wave of wavelength $4\mathbf{r}_0$ propagating in the $\mathbf{r}_0$ direction (Fig. 2a). In Fig. 2b,

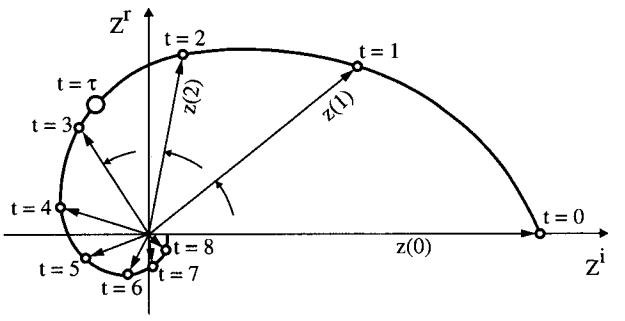

FIG. 1. Schematic diagram of the time evolution of POP coefficients $z(t)$ with an initial value $z(0) = (z^r, z^i) = (0, 1)$. The complex number z rotates in slightly more than eight time steps anticlockwise once around the origin so that the period T is slightly larger than eight time steps. The e-folding time τ, for which $|z(\tau)| = 1/e$ is marked by an open circle. (From von Storch et al. 1990.)

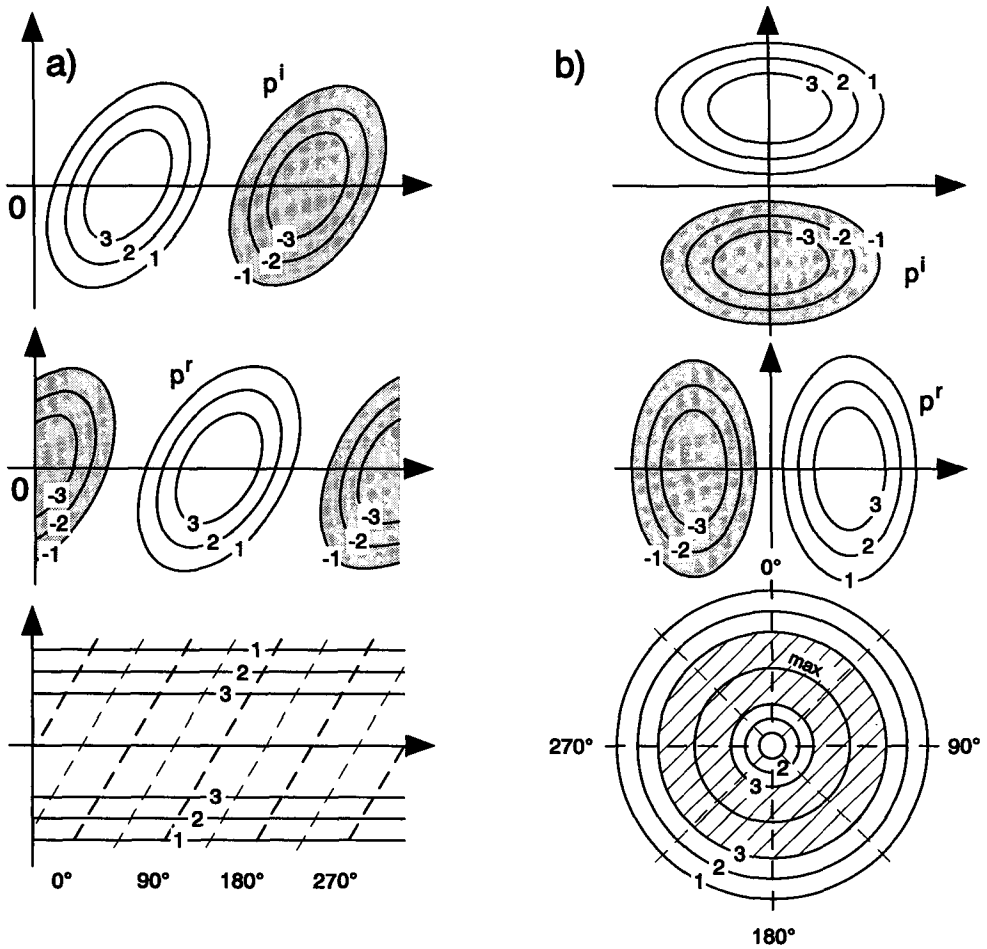

FIG. 2. Schematic examples representating a complex valued POP $\mathbf{p} = \mathbf{p}^r + i\mathbf{p}^i$ by their imaginary parts $\mathbf{p}^i$ (top) and their real parts ($\mathbf{p}^r$ (middle), and by their phases (ψ) and amplitudes A (bottom). In the left column (a), a linearly propagating wave is displayed. If the system is initially $\mathbf{P} = 1 \cdot \mathbf{p}^i$ (top), then after a quarter of a period it will be in the state $\mathbf{P} = 1 \cdot \mathbf{p}^r$ (middle). The wave propagates to the right with a constant phase speed (bottom), and the amplitude is constant along horizontal lines with maximum values in the center. In the right column (b), a rotational wave is shown. With the origin of the plane being between the two features in the top two diagrams, the wave rotates clockwise around this origin. In the center the amplitude is always zero, and the lines of constant amplitudes form concentric circles around the center with a maximum somewhat off the center. (From von Storch et al. 1988.)

an amphidromal (rotational) wave[1] is shown. In the present paper, all POPs are represented in the $\mathbf{p}^i/\mathbf{p}^r$ format and not in the amplitude–relative phase format.

The pattern coefficients z_j are given as the dot product of $\mathbf{x}$ with the *adjoint patterns* $\mathbf{p}_j^A$, which are the normalized eigenvectors of $\mathcal{A}^T$:

$$(\mathbf{p}_j^A)^T\mathbf{x} = \sum_k z_k(\mathbf{p}_j^A)^T\mathbf{p}_k = z_j. \qquad (8)$$

All information used so far consists of the existence of a linear equation (1) with some matrix $\mathcal{A}$. No assumption was made as to from where this matrix originates. In dynamical theory, the origins of (1) are linearized and discretized differential equations. In case of the POP analysis, the relationship

$$\mathbf{x}(t+1) = \mathcal{A} \cdot \mathbf{x}(t) + \text{noise} \qquad (9)$$

is hypothesized. Multiplication of (9) from the right-hand side by the transposed $\mathbf{x}^T(t)$ and taking expectations E leads to

$$\mathcal{A} = E[\mathbf{x}(t+1)\mathbf{x}^T(t)] \cdot [E[\mathbf{x}(t)\mathbf{x}^T(t)]]^{-1}. \qquad (10)$$

The eigenvectors of (10), or the normal modes of (9), are called *principal oscillation patterns*. The coefficients z are called *POP coefficients*. Their time evolution is given by (3), superimposed by noise:

$$z(t+1) = \lambda \cdot z(t) + \text{noise}. \qquad (11)$$

[1] An amphidromal wave is a propagating wave that circles clockwise or anticlockwise around a center that is always at rest. Many tidal waves appear as amphidromal waves.

The stationarity of (11) requires $\rho = |\lambda| < 1$. In practical situations, when only a finite time series $\mathbf{x}(t)$ is available, $\mathcal{A}$ is estimated by first deriving the sample lag-1 covariance matrix $\mathcal{X}_1 = E[\mathbf{x}(t+1)\mathbf{x}^{\mathrm{T}}(t)]$ and the sample covariance matrix $\mathcal{X}_0 = E[\mathbf{x}(t)\mathbf{x}^{\mathrm{T}}(t)]$, and then forming $\mathcal{A} = \mathcal{X}_1\mathcal{X}_0^{-1}$. The eigenvalues of this matrix always satisfy $\rho < 1$.

Since no data compression mechanism is incorporated into the POP analysis, the data are often subjected to a truncated EOF expansion in order to reduce the number of spatial degrees of freedom. In this case, the POP analysis is applied to the vector of the first few EOF coefficients. A positive by-product of this procedure is that in this way noisy components can be excluded from the analysis. Then, the covariance matrix $\mathcal{X}_0$ has a diagonal form.

If there is a priori information that the expected signal is located in a certain frequency band, it is often advisable to time filter the data prior to the POP analysis. A somewhat milder form of focusing on selected timescales is to derive the EOFs from time-filtered data, but then to project the unfiltered data onto these EOFs.

We have seen that, in the theoretical framework for complex normal modes, the real and imaginary parts $z^r(t)$ and $z^i(t)$ vary coherently with a frequency of $\eta = 2\pi/T$ and a phase lag of $\pi/2$ [with z^r lagging z^i; see (7) and (8)]. Since POPs and their corresponding coefficient time series $z(t)$ (11) are empirically derived modes, it has to be verified that $z(t)$ behaves in a similar way in order to be interpreted in this same framework. This can be accomplished by performing a cross-spectral analysis of the real part $z^r(t)$ and the imaginary part $z^i(t)$ of the POP coefficients. If, in the neighborhood of the period η, both parts exhibit large values in the variance spectrum accompanied with a large coherence and a phase spectrum close to $\pi/2$, then $z^r(t)$ and $z^i(t)$ do indeed vary coherently and can be interpreted in the sense of (7) and the cycle (8) (see Fig. 3c for an example). Complex POPs not fulfilling these conditions cannot be interpreted in this framework of oscillating patterns and are disregarded.

If the original time series $\mathbf{x}(t)$ is transformed into another time series $\mathbf{y}(t)$ by means of $\mathbf{y}(t) = \mathcal{L} \cdot \mathbf{x}(t)$ with an invertible matrix $\mathcal{L}$ (i.e., $\mathcal{L}^{-1}$ exists), then the eigenvalues are unchanged and the eigenvectors transform as x:

$$\mathcal{A}_X = \mathcal{X}_1\mathcal{X}_0^{-1};\ \mathcal{A}_Y = \mathcal{Y}_1\mathcal{Y}_0^{-1}$$

with $\mathcal{Y}_1 = E(\mathbf{y}(t+1)\mathbf{y}(t)^{\mathrm{T}}) = \mathcal{L}\mathcal{X}_1\mathcal{L}^{\mathrm{T}}$ and $\mathcal{Y}_0 = \mathcal{L}\mathcal{X}_0\mathcal{L}^{\mathrm{T}}$. Thus, $\mathcal{A}_Y = \mathcal{L}\mathcal{A}_x\mathcal{L}^{-1}$. If $\mathbf{p}_x$ is an eigenvector of $\mathcal{A}_x$ with eigenvalue λ (i.e., $\mathcal{A}_x\mathbf{p}_x = \lambda\mathbf{p}_x$), then $\mathcal{A}_x\mathcal{L}^{-1}\mathcal{L}\mathbf{p}_x = \lambda\mathbf{p}_x$ and, eventually, $\mathcal{L}\mathcal{A}_x\mathcal{L}^{-1} \times (\mathcal{L}\mathbf{p}_x) = \lambda(\mathcal{L}\mathbf{p}_x)$. That is, if $\mathbf{p}_x$ is a POP of the time series $\mathbf{x}$, then $\mathcal{L}\mathbf{p}_x = \mathbf{p}_Y$ is a POP of $\mathbf{y}$ with the same eigenvalue λ.

The EOFs are not invariant against linear transformations $\mathcal{L}$, since, in general, the matrices $\mathcal{X}_0$ and $\mathcal{L}\mathcal{X}_0\mathcal{L}^{\mathrm{T}}$ will have different eigenvalues and eigenvectors. Therefore, if the POP analysis is begun with a projection of the data on a truncated EOF expansion, the results of a POP analysis will change if the data are transformed into another coordinate system.

To get the POP coefficients $z(t)$, two approaches are possible. One is to derive the adjoint patterns $\mathbf{p}^{\mathrm{A}} = \mathbf{p}^{\mathrm{A},r} + i\mathbf{p}^{\mathrm{A},i}$ and to use (8). The adjoint patterns can be estimated as the eigenvectors of the estimated matrix $\mathcal{A}^{\mathrm{T}}$. This is not always a stable procedure as the eigenvectors $\mathbf{p}^{\mathrm{A}}$ of the estimated matrix $\mathcal{A}^{\mathrm{T}}$ have to satisfy the constraint $[\mathbf{p}_i^{\mathrm{A}}]^{\mathrm{T}}\mathbf{p}_j = \delta_{ij}$. Thus, the adjoint of the POP of interest *has to be orthogonal to all other POPs*, and in particular, to those POPs that are merely reflecting noise. Therefore, it is often advisable to estimate the patterns $\mathbf{p}^{\mathrm{A}}$ by minimizing

$$\|\mathbf{x} - [\mathbf{x}^{\mathrm{T}}\mathbf{p}^{\mathrm{A}}]\mathbf{p}\|, \tag{12}$$

if $\mathbf{p}$ is real, or

$$\|\mathbf{x} - [\mathbf{x}^{\mathrm{T}}\mathbf{p}^{\mathrm{A},r}]\mathbf{p}^r - [\mathbf{x}^{\mathrm{T}}\mathbf{p}^{\mathrm{A},i}]\mathbf{p}^i\|, \tag{13}$$

if $\mathbf{p} = \mathbf{p}^r + i\mathbf{p}^i$ is complex. The minimum of (12) is obtained at

$$\mathbf{p}^{\mathrm{A}} = \frac{1}{[\mathbf{p}^{\mathrm{T}}\mathbf{p}]}\,\mathbf{p} \tag{14}$$

and the minimum of (13) is at

$$\begin{pmatrix}\mathbf{p}^{\mathrm{A},r}\\ \mathbf{p}^{\mathrm{A},i}\end{pmatrix} = \kappa\begin{pmatrix}\dfrac{1}{\mathbf{p}^{r\mathrm{T}}\mathbf{p}^r}\,\mathbf{p}^r & -\dfrac{1}{\mathbf{p}^{r\mathrm{T}}\mathbf{p}^i}\,\mathbf{p}^i\\ \dfrac{1}{\mathbf{p}^{i\mathrm{T}}\mathbf{p}^i}\,\mathbf{p}^i & -\dfrac{1}{\mathbf{p}^{r\mathrm{T}}\mathbf{p}^i}\,\mathbf{p}^r\end{pmatrix} \tag{15}$$

with

$$\kappa = ([\mathbf{p}^{r\mathrm{T}}\mathbf{p}^r]\cdot[\mathbf{p}^{i\mathrm{T}}\mathbf{p}^i] - [\mathbf{p}^{r\mathrm{T}}\mathbf{p}^i]^2)^{-1}. \tag{16}$$

An alternative is to not derive adjoint patterns but to derive the coefficients z by a least-square fit of the data $\mathbf{x}$ by minimizing

$$\|\mathbf{x} - z\cdot\mathbf{p} - [z\cdot\mathbf{p}]^*\| = \|\mathbf{x} - z^r\mathbf{p}^r - z^i\mathbf{p}^i\| \tag{17}$$

if $\mathbf{p}$ is complex, or

$$\|\mathbf{x} - z\cdot\mathbf{p}\| \tag{18}$$

if $\mathbf{p}$ is real. The solution of (17) is

$$\begin{pmatrix}\mathbf{p}^{r\mathrm{T}}\mathbf{p}^r & \mathbf{p}^{r\mathrm{T}}\mathbf{p}^i\\ \mathbf{p}^{r\mathrm{T}}\mathbf{p}^i & \mathbf{p}^{i\mathrm{T}}\mathbf{p}^i\end{pmatrix}\cdot\begin{pmatrix}z^r\\ z^i\end{pmatrix} = \begin{pmatrix}\mathbf{x}^{\mathrm{T}}\mathbf{p}^r\\ \mathbf{x}^{\mathrm{T}}\mathbf{p}^i\end{pmatrix}, \tag{19}$$

and the solution of (18) is, formally, the regression of $\mathbf{x}$ on $\mathbf{p}$:

$$z(t) = \frac{\mathbf{x}(t)^{\mathrm{T}}\cdot\mathbf{p}}{\mathbf{p}^{\mathrm{T}}\cdot\mathbf{p}}. \tag{20}$$

The solutions (17), (18) may be rewritten as $z = \mathbf{x}^{\mathrm{T}}\mathbf{q}$ with a certain complex or real pattern $\mathbf{q}$. Incidentally, $\mathbf{q} = \mathbf{p}^{\mathrm{A},r} + i\mathbf{p}^{\mathrm{A},i}$ or $\mathbf{q} = \mathbf{p}^{\mathrm{A}}$. Thus, the minimizations

of (12), (13) and of (17), (18) yield the same POP coefficients z.
If the POP coefficients are obtained by (12), (13), (2) is no longer valid. Therefore, if more than one POP is identified as useful, the equations (17), (18) should be formulated for all considered POPs $\mathbf{p}_j$ simultaneously: $\|\mathbf{x} - \sum_j z_j \mathbf{p}_j\| = \min$.

b. POPs as multivariate spectral analysis

The autospectrum Γ_z of the POP coefficients $z(t)$ is a function of the eigenvalue λ and of the autospectrum Γ_n of the noise [see (11)]:

$$\Gamma_z(\omega) = \frac{\Gamma_n(\omega)}{|e^{i\omega} - \lambda|^2}, \tag{21}$$

where ω is frequency.

If the noise spectrum Γ_n is almost white, that is, $\Gamma_n(\omega) \approx$ const, the left-hand side of (21) does depend only on λ. In this case, the eigenvalue λ is thus representative for the temporal statistics of the signal, expressed through the autospectrum Γ_z. We will assume $\Gamma_n(\omega) = 1$ for the remainder of this subsection.

The width of the spectrum depends on ρ. The smaller ρ is the broader is the spectrum (in the limit of $\rho = 0$ the spectrum is white). The spectrum Γ_z has a single maximum $\Gamma_z = (1 - \rho)^{-2}$ at $\omega = \eta$. If λ is complex, then $\eta \neq 0$; if λ is real, then $\eta = 0$ and the spectrum is red.

Thus, the POP analysis yields a multivariate spectral analysis of a vector time series (Hasselmann 1988). A first attempt to simultaneously derive several signals with different spectra from a high dimensional dataset was made by Xu (1993).

c. POPs = trivial case of PIPs

Many complex dynamical systems $\mathbf{x} \in \mathbf{R}^n$ may conveniently be approximated as being driven by a simpler dynamical system $\mathbf{z} \in \mathbf{R}^m$ with a reduced number of degrees of freedom $m \leq n$. Mathematically, this may be described by a *state space model,* which consists of a *system* equation,

$$\mathbf{z}(t+1) = \mathcal{F}[\mathbf{z}(t), \alpha, t] + \text{noise} \tag{22}$$

for the dynamical variables $\mathbf{z} = (z_1, \cdots, z_m)$, and an *observation* equation,

$$\mathbf{x}(t) = \mathcal{P}\mathbf{z}(t) + \text{noise} = \sum_j z_j(t)\mathbf{p}_j + \text{noise} \tag{23}$$

for the observed variables $\mathbf{x}$; $\mathcal{P}$ is the matrix whose columns are the vectors, or *patterns,* $\mathbf{p}_j$. In general, $\mathcal{P}$ is not a square matrix. In (22) $\mathcal{F}[\mathbf{z}(t), \alpha, t]$ denotes a class of models that can be nonlinear in the dynamical variables $\mathbf{z}$ and additionally depends on a set of free parameters $\alpha = (\alpha_1, \alpha_2, \cdots)$. Both equations, (22), (23), are disturbed by an additive noise. Formulation (22), (23) is an "inverse modeling" approach.

Since $m \leq n$, the time coefficients $z_j(t)$ of a pattern $\mathbf{p}_j$ at a time t are not uniquely determined by the $\mathbf{x}(t)$. Instead, they may be obtained by a least-square fit; that is,

$$\mathbf{z}(t) = (\mathcal{P}^T\mathcal{P})^{-1}\mathcal{P}^T\mathbf{x}(t). \tag{24}$$

The intriguing aspect of state space models is that the dynamical behavior of complex systems often appears to be dominated by the interaction of only a few characteristic patterns $\mathbf{p}_j$. That is, even if the dynamics of the full system are restricted to the subspace spanned by the columns of $\mathcal{P}$, its principal dynamical properties are represented.

When fitting the state space model (22), (23) to a time series, the following entities have to be specified: the class of models $\mathcal{F}$, the patterns $\mathcal{P}$, the free parameters α, and the dimension of the reduced system m. The class of models $\mathcal{F}$ has to be selected a priori on the basis of physical reasoning. Also, the number m might be specified a priori. The parameters α and the patterns $\mathcal{P}$ are fitted simultaneously to a time series by requesting them to minimize

$$\epsilon[\mathcal{P}; \alpha] = E\|\mathbf{x}(t+1) - \mathbf{x}(t) - \mathcal{P}(\mathcal{F}[\mathbf{z}(t), \alpha, t] - \mathbf{z}(t))\|^2, \tag{25}$$

where $\epsilon[\mathcal{P}; \alpha]$ is the mean-square error of the approximation of the (discretized) time derivative of the observations $\mathbf{x}$ by the state space model. The patterns $\mathcal{P}$, which minimize (25), are called *principal interaction patterns* (Hasselmann 1988). If only a finite time series of observations $\mathbf{x}$ is available, the expectation E is replaced by a summation over time.

In general, the minimization of (25) is not unique. In particular, the set of patterns $\mathcal{P}' = \mathcal{P} \cdot \mathcal{L}$ with any nonsingular square matrix $\mathcal{L}$ will minimize (25), if $\mathcal{P}$ does, as long as the corresponding model $\mathcal{F}' = \mathcal{L}^{-1}\mathcal{F}$ belongs to the a priori specified model class. This problem may be solved by requesting the solution to fulfill some constraints; for example, that the linear term in the Taylor expansion of $\mathcal{F}$ be a diagonal matrix.

So far, the PIP concept has not been fully implemented, but encouraging progresses are reported from several groups. There are, though, a number of partial implementations of the PIPs in which the basic model is simplified. In the case reported by von Storch et al. (1990), the basic model is linear with cyclostationary coefficients; also Penland's approach may be seen as a linear PIP approach (Penland 1989; Penland and Ghil 1993; Penland and Magorian 1993). The most significant progress toward full implementation has been obtained by Selten (1995), who fitted the dynamics of the nonlinear barotropic vorticity equation, with only 20 degrees of freedom, to the first 20 EOFs of the flow. In this case, only the unknown parameters α in (22) were derived from the data, whereas the patterns $\mathcal{P}$ were specified a priori as EOFs.

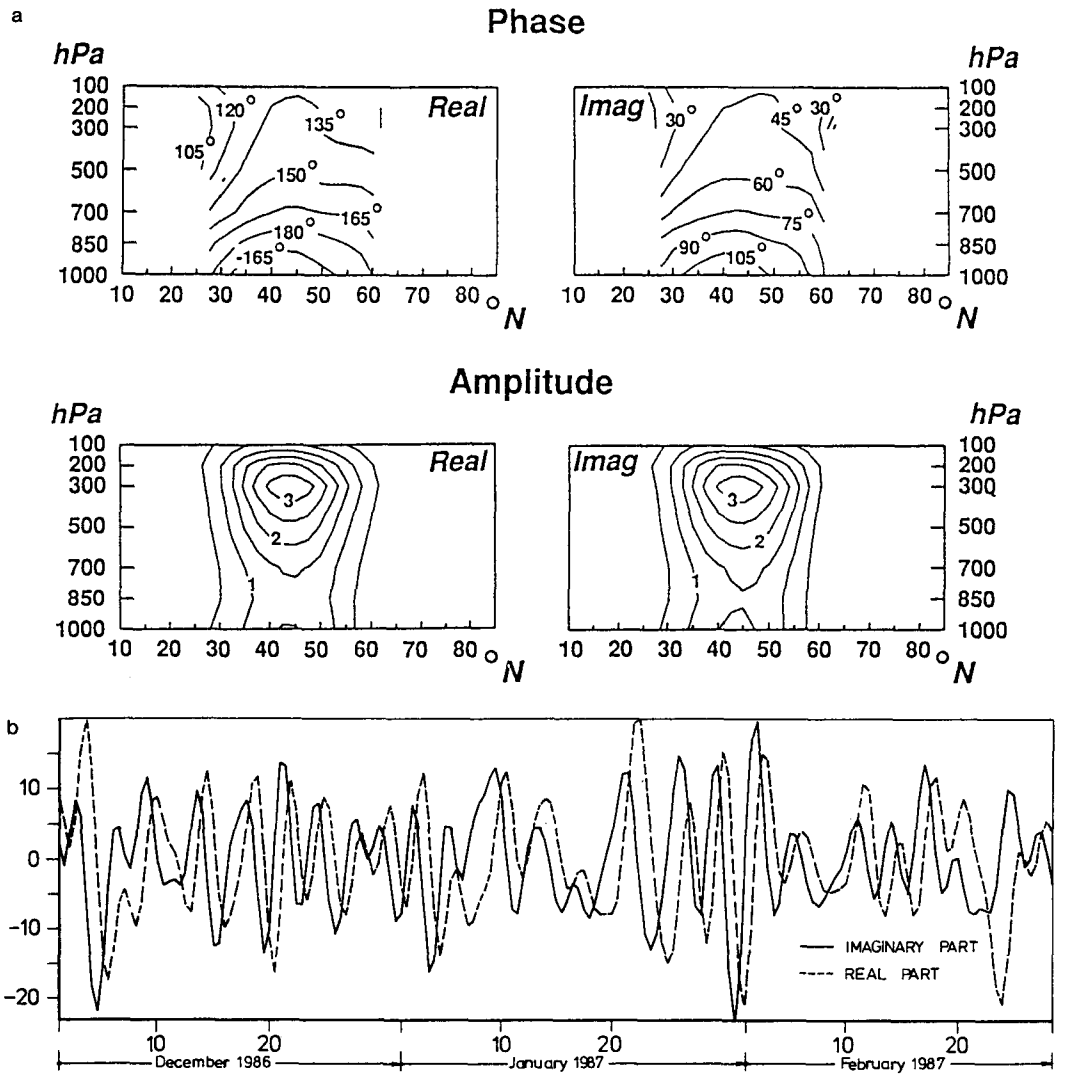

FIG. 3. Baroclinic waves: The POP $\mathbf{p}$ of a POP analysis of twice-daily geopotential height in the Northern Hemisphere for zonal wavenumber $k = 8$, which explains a maximum (54%) of variance. The oscillation period T is 4 days and the e-folding time is 8.1 days. For more information see Section 3a. The POPs tend to appear in sequences $\cdots \rightarrow \mathbf{p}^r \rightarrow -\mathbf{p}^i \rightarrow -\mathbf{p}^r \rightarrow \mathbf{p}^i \rightarrow \mathbf{p}^r \rightarrow \cdots$; dimensionless units. (a) The patterns $\mathbf{p}^r = \mathrm{Re}(\mathbf{p})$ (left) and $\mathbf{p}^i = \mathrm{Im}(\mathbf{p})$ (right) represented by their amplitude patterns $\mathbf{A}^r$ and $\mathbf{A}^i$ (bottom) and phase patterns Θ^r and Θ^i (top). The absolute values of the amplitudes are arbitrary since POPs are always normalized. The phase lines are only plotted where the amplitude is at least 6% of its maximum value. (From Schnur et al. 1993.) (b) The coefficient time series z^r (dashed) and z^i (solid). Note that, in contrast to Schnur et al. (1993), this coefficient time series was derived as a least-square fit through (17). (c) Cross-spectral analysis between z^r and z^i. The vertical dashed line marks the POP period T, and the horizontal dashed lines in the coherence plot denote the confidence limits for the respective percentage values testing the null hypothesis of zero coherence.

The POPs can be understood as a kind of simplified PIPs. For that, assume $m = n$. Then, the patterns $\mathcal{P}$ span the full $\mathbf{x}$ space and their choice does not affect $\epsilon[\mathcal{P}; \alpha]$. Also, let $\mathcal{F}$ be a linear model $\mathcal{F}[\mathbf{z}(t), \alpha] = \mathcal{A} \cdot \mathbf{z}(t)$, where the parameters α are the entries of $\mathcal{A}$. Then the dynamical equation (22) is identical to (11). The constraint mentioned above leads to the eigenvectors of $\mathcal{A}$ as being the PIPs of the particular, admittedly simplified, state space model.

When we relate the definition of POPs, as given in section 2a, to the PIPs, as given by equations (22), (23) and the minimization (25), we have to assume $m = n$. That is, the POP approach does not automatically deliver a reduction of the degrees of freedom of the considered phase space. Instead, a POP analysis results in the identification of relevant modes. It is for this reason that we used the expression "trivial" in the heading of this subsection.

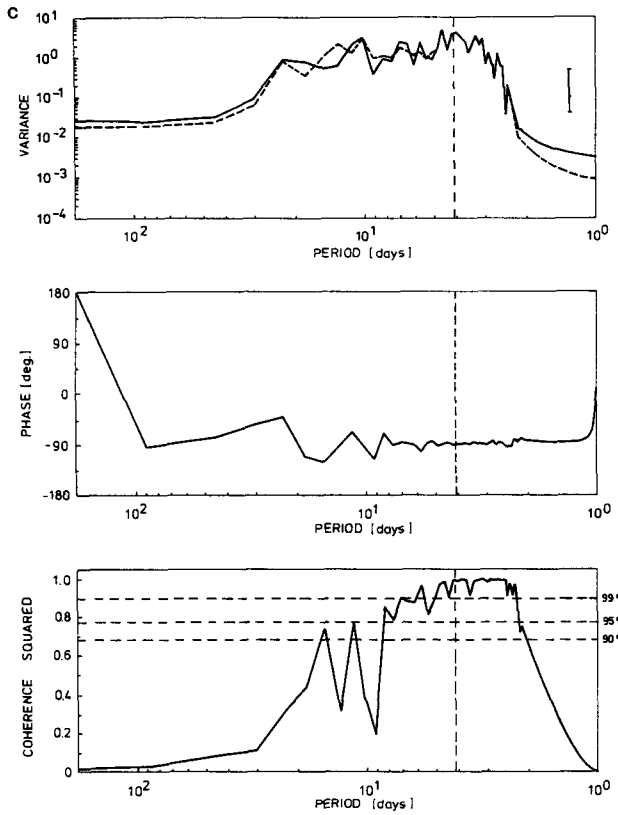

FIG. 3. (*Continued*)

The approach of Penland and coworkers (Penland 1989; Penland and Ghil 1993; Penland and Magorian 1993), on the other hand, pursues the original "linear inverse modeling" idea of the PIPs, and the use of the expression "POPs" in both contexts has created some confusion.

3. Examples

a. Tropospheric Rossby waves given by POP analysis and stability analysis

POPs can be seen as normal modes of a linear approximation to a system, the dynamics of which are unknown or too complex to be described exlicitly. A conceptually different approach to the derivation of normal modes is to consider a linearization of a possibly complex set of dynamical equations and to compute the corresponding eigenmodes.

These two concepts are compared in the context of tropospheric baroclinic waves, which are responsible for much of the high-frequency atmospheric variability in midlatitudes. For this purpose, a POP analysis with twice-daily geopotential heights Ψ at various tropospheric levels and a conventional linear stability analysis of the quasigeostrophic vorticity equation were performed (Schnur et al. 1993). For both analyses the signals are expected to propagate mostly in the zonal direction on top of a zonally symmetric mean state, so that waves may conveniently be described by a semi-spectral representation:

$$\Psi(\lambda, \phi, z, t) = \Psi_1(\phi, z, t)\cos(k\lambda) + \Psi_2(\phi, z, t)\sin(k\lambda) \quad (26)$$

with λ longitude, ϕ latitude, z height, and k the zonal wavenumber. A pair Ψ_1, Ψ_2 of zonal Fourier coefficients is equivalent to a complex coefficient $a\exp(i\theta)$ of $\exp(-ik\lambda)$ representing the zonal wave (26) by

$$a\cos(k\lambda - \theta) = Re[a\exp i(\theta - k\lambda)] \quad (27)$$

with an amplitude $a = a(\phi, z, t)$ and a phase $\theta = \theta(\phi, z, t)$. This representation is used in the diagrams.

1) POP ANALYSIS

In the POP analysis, the state vector $\mathbf{X}$ is formed from the data for each wavenumber separately by the trigonometric coefficients Ψ_1 and Ψ_2 of geopotential height at all latitudes and heights. The system matrix $\mathcal{A}$ of (1) is estimated from the European Centre for Medium-Range Weather Forecasts analyses for the winters (DJF) 1984/85 through 1986/87.

There is a preconception on the timescale so that the time series for the POP analysis are bandpass filtered retaining all variability between 3 and 25 days. Also, an EOF expansion was made prior to the POP analysis retaining the first 18 EOFs, which explain more than 95% of the total variance for each wavenumber. Repetition of some analyses with fewer EOFs showed, however, that the characteristics of the most important POPs are not very sensitive to the number of EOFs retained.

Here, only one POP obtained for the zonal wavenumber 8 on the Northern Hemisphere is discussed (Fig. 3). The POP explains 54% of the wavenumber $k = 8$ variance and has a period $T = 4.0$ days and a damping time $\tau = 8.1$ days. Note that the decay time is sensitive to the type of time filter.

Since, at any time t, the vector of state $\mathbf{x}$ is formed by the sine and cosine coefficients of the zonal geopotential height waves, both real and imaginary parts of the complex POP, $\mathbf{p} = \mathbf{p}^r + i\mathbf{p}^i$, have to be interpreted also as a vector of sine and cosine coefficients, which can be represented by amplitude patterns $\mathbf{A}^r = [a^r(\phi, z)]$ and $\mathbf{A}^i = [a^i(\phi, z)]$ and phase patterns $\mathbf{\Theta}^r = [\theta^r(\phi, z)]$ and $\mathbf{\Theta}^i = [\theta^i(\phi, z)]$.

These are shown in Fig. 3a as height–latitudinal distributions. Note that if we considered the phases and amplitudes at a fixed height as a function of latitude only and expanded each amplitude/phase pair ($\mathbf{A}^r/\mathbf{\Theta}^r$ resp. $\mathbf{A}^i/\mathbf{\Theta}^i$) back to a wave in physical latitude–longitude space, we would get a picture as in the upper part of Fig. 2a. [cf. Fig. 6 in Schnur et al. (1993) for the 200-hPa cross section] (in interpretating the figure

it might be useful to move along horizontal or vertical cross sections, in one's mind's eye, fixing the respective other dimension). It should be noted that also in this case the complex POP is represented by its real and imaginary patterns (top two rows of Fig. 2) as opposed to the representation by means of relative phases and amplitudes ψ [in the lower row of Fig. 2; see discussion after (7)]. Here, the complex POP just happens to consist of phases and amplitudes of three-dimensional waves such that the real and imaginary parts themselves are shown as amplitudes and phases.

As can be seen in Fig. 3a, the amplitude fields $\mathbf{A}^r$ and $\mathbf{A}^i$ are almost identical, and the phase distribution Θ^r is shifted by 90° relative to the phase distribution Θ^i at those latitudes where the amplitudes are significant. This information, together with the interpretation (7), leads to the conclusion that the considered POP describes an eastward traveling pattern.

The coefficient time series $z^r(t)$ and $z^i(t)$ was obtained as a least-squares fit to the POPs (17) at each half-day t in all winter (Fig. 3b). The two curves vary coherently, with $z^r(t)$ lagging $z^i(t)$ by one or two days. This visual finding is substantiated by the cross-spectral analysis of the two coefficient time series (Fig. 3c). Maximum variance is at timescales of 3 to 5 days, the phase difference is uniformly 90°, as it should be, and the coherence is very high in the neighborhood of the POP period of 4 days.

2) INSTABILITY ANALYSIS

In the instability analysis the quasigeostrophic vorticity equation on a sphere is linearized around the observed zonally averaged mean winter state and discretized. Using representation (26) for the streamfunction Ψ for each wavenumber k and forming the (unknown) state vector $\mathbf{x}$ from Ψ_1 and Ψ_2 as above, the system equation is of the form (1) where the system matrix $\mathcal{A}$ is known from theoretical reasoning.

Now (1) has complex eigensolutions $\mathbf{Q} = \mathbf{Q}^r + \mathbf{Q}^i$. The complex eigenvalue, which is connected with the pattern $\mathbf{Q}$, is equivalent to an amplifying, or damping, rate and to a period T. Thus, apart from the amplification or damping, the normal modes again appear in a cyclic sequence (7) representing propagating waves. The phase direction depends on the eigenvalue λ. For the following discussion, it is useful to rewrite (6) in terms of the e-folding time $\tau = -1/\ln(|\lambda|)$:

$$\mathbf{P}(t) = e^{-t/\tau}[\cos(\eta t)\cdot \mathbf{p}^r - \sin(\eta t)\cdot \mathbf{p}^i].$$

The term e-folding time will be used here in a more general sense in that it describes both damping ($\tau > 0$) as well as amplifying ($\tau < 0$) solutions, corresponding to $|\lambda| < 1$ and $|\lambda| > 1$, respectively. A positive e-folding time is the time required to damp an initial unit amplitude to $1/e$, and a negative e-folding represents the time until a growing amplitude is increased from 1 to e. With this terminology in mind, the following difference between the POP analysis and the stability analysis with respect to the e-folding time should be noted.

As mentioned before, the POP analysis of stationary data always yields eigenvalues $\lambda \leqslant 1$, because any eigenvalue with $\lambda > 1$ would characterize an exploding, and therefore nonphysical, solution. By estimating the matrix $\mathcal{A}$ of the linear system (1) from the data, the POP analysis preferentially "sees" an oscillation in its mature state when noise is relatively small and damping occurs because of nonlinear and other processes. The e-folding time $\tau = -1/\ln(|\lambda|)$ gives a statistical measure of how long, on the average, such a signal is seen before noise, which reflects both stochastic noise as well as unknown and nonlinear dynamical processes, becomes more and more important. In this sense the e-folding time characterizes the statistical significance of a POP.

In the stability analysis the system matrix $\mathcal{A}$ is derived from a linearization of a nonlinear dynamical equation where a small perturbation is superimposed on a basic state. This system contains the potential of amplifying solutions and, actually, these are the solutions we are interested in. Thus, in this case eigenvalues with $\lambda \geqslant 1$ describe the formation and growth ($\tau < 0$) of oscillations, which the POP analysis eventually detects. Here, the e-folding is equivalent to an amplification rate where a normal mode with a larger growth rate is considered more significant than a mode with a smaller growth rate. This interpretation is based on the assumption that the fastest growing modes will emerge first from a background of many perturbations any initial condition consists of.

Like the POPs, both $\mathbf{Q}^r$ and $\mathbf{Q}^i$ represent an amplitude pattern and a phase pattern. However, since the system matrix depends only on a zonally averaged basic state, the solutions have to be invariant against zonal rotation (unlike the POPs). It can be shown that the amplitudes of patterns $\mathbf{Q}^r$ and $\mathbf{Q}^i$ coincide and that the phase of $\mathbf{Q}^i$ is just the phase of $\mathbf{Q}^r$ shifted by −90°; that is, the pattern $\mathbf{Q}^i$ is redundant and only the amplitude $\mathbf{A}^q$ and the phase Θ^q of $\mathbf{Q}^r$ have to be considered.

The most unstable normal mode obtained for wavenumber 8 on the Northern Hemisphere has a period of $T = 3.9$ days. It is amplifying so that an initial unit amplitude has grown by a factor of e after 2.2 days. The mode is propagating eastward.

The amplitude pattern $\mathbf{A}^q$ (Fig. 4) of this normal mode is almost identical to the amplitude patterns of the POP shown in Fig. 3a: $\mathbf{A}^q \approx \mathbf{A}^r \approx \mathbf{A}^i$. A difference is the maximum of the normal mode at the bottom, which can be attributed to the omission of friction in the stability analysis. The phase pattern Θ^q differs from the POP phases $\Theta^r \approx \Theta^i - \pi/2$ only by a constant angle. The phase depends only weakly on latitude, indicating almost no meridional momentum transport. In the vertical, the mode exhibits a small westward tilt.

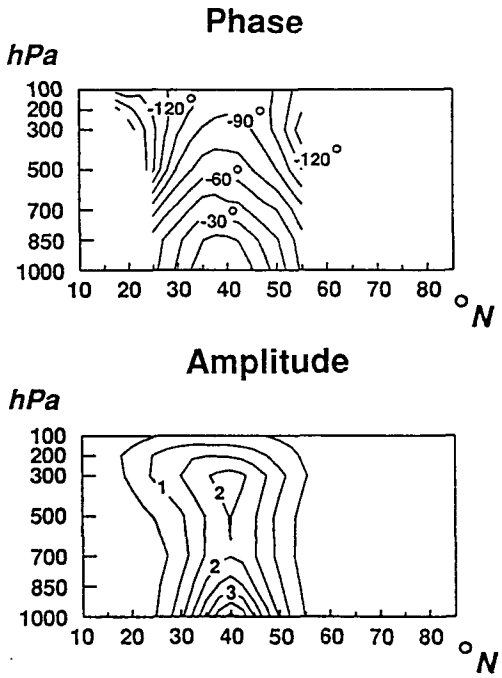

FIG. 4. Baroclinic waves: The patterns $\mathbf{Q}^r$ and $\mathbf{Q}^i$ of the most unstable zonal wavenumber 8 mode on the Northern Hemisphere identified in stability analysis of the discretized quasigeostrophic vorticity equation linearized about the observed zonal mean state in northern winter. The e-folding growth rate is 2.2 days and the period T is 3.9 days. Since the unstable mode is completely determined by the real part only, the amplitude and phase pattern $\mathbf{A}^q$ (bottom) and Θ^q (top) of $\mathbf{Q}^r$ have to be shown; $\mathbf{Q}^i$ is then given by $\mathbf{A}^q$ and $\Theta^q - \pi/2$. (From Schnur et al. 1993.)

The time coefficients $z^r(t)$ and $z^i(t)$ can again be calculated as a least-squares fit to the two patterns $\mathbf{Q}^r$ and $\mathbf{Q}^i$ (not shown). These coefficients explain 38% of the wavenumber 8 variance. The cross-spectrum (not shown) between $z^r(t)$ and $z^i(t)$ is similar to the cross-spectrum of the POP coefficients (Fig. 3c). There is maximum variance, a phase difference of 90°, and a high coherence at the theoretical period $T = 3.9$ days.

Figure 5 shows the result of a complex cross-spectral analysis between the POP coefficient time series (Fig. 3b) and the coefficient time series of the unstable normal mode. The variance of both time series has a maximum at a frequency of -0.25 (the negative sign corresponds to an eastward progression of the respective patterns) where also the coherence is very high and the phase is fairly flat. This shows that both modes oscillate coherently at a common period of 4 days, thus representing the same feature in the geopotential height fields. Note that the value of the phase is not of importance here because it only reflects the different absolute values in the phase patterns of the POP and the unstable mode, respectively (Figs. 3a and 4).

Summarizing, the POP analysis, which estimates the system matrix of a linear system from observation data, finds similar modes as conventional stability analysis, which makes use of first-principle dynamical reasoning to obtain the matrix. Thus, the POP patterns can be attributed to the linear growing phase in the life cycle of baroclinic waves.

Results, not discussed here, also indicate that in contrast to the instability analysis the POP analysis is also able to identify oscillations that may be connected to the (nonlinear) decay phase in the life cycle of baroclinic unstable modes (Schnur et al. 1993). If the POP analysis is done simultaneously for all zonal wavenumbers 5–9 (Schnur 1993), the resulting patterns are also in very good agreement to three-dimensional instability analyses, which use a zonally asymmetric basic state (e.g., Frederiksen 1982). The most significant patterns reflect the storm track regions connected with the inhomogeneity of the atmospheric flow, especially in the Northern Hemisphere.

b. The Southern Oscillation and the quasi-biennial oscillation

Two oscillations in the tropical atmosphere with similar oscillation period—the stratospheric *quasi-biennial oscillation* (QBO) and the tropospheric Southern Oscillation—and the relationship between these two oscillations are examined by means of the POP analysis (Xu 1992).

The QBO is reflected in the equatorial zonal wind of which time series are available at six stratospheric levels. In the POP analysis deviations from the long-term mean are considered. No time filtering was done for this dataset.

Monthly mean anomalies along the equator (50°E–80°W) of the 10-m zonal wind and of the sea surface temperature (SST) anomalies are used to describe the SO signal. To remove high frequency noise the time series are low-pass filtered. All variability on timescales less than 15 months is suppressed.

One POP analysis is performed to simultaneously analyze the three equatorial datasets: stratospheric wind, zonal surface wind, and SST. The three components are normalized so that they contribute an equal amount of variance to the combined dataset.

Two significant POP pairs (Fig. 6) are found, one with an oscillation period $T = 28$ mo and the other with $T = 45$ mo. The cross-spectral analysis of the POP coefficients (not shown) indicates that the 28-mo period of the first POP is reliably estimated, but that the period of $T = 45$ mo of the second POP is overestimated. A more adequate value for the period would be about 30 mo, since the coherence spectrum has a maximum at the frequency $2\pi/30$ mo.

Mode 1 is significant only in the stratosphere (right panel of Fig. 6a), where it represents the downward propagation of a signal from the uppermost level to the lower stratosphere (the heavy lined $\mathbf{p}^i$ leads, according to (7), the light lined $\mathbf{p}^r$) within 14 months. The POP coefficients time series (not shown) oscillate

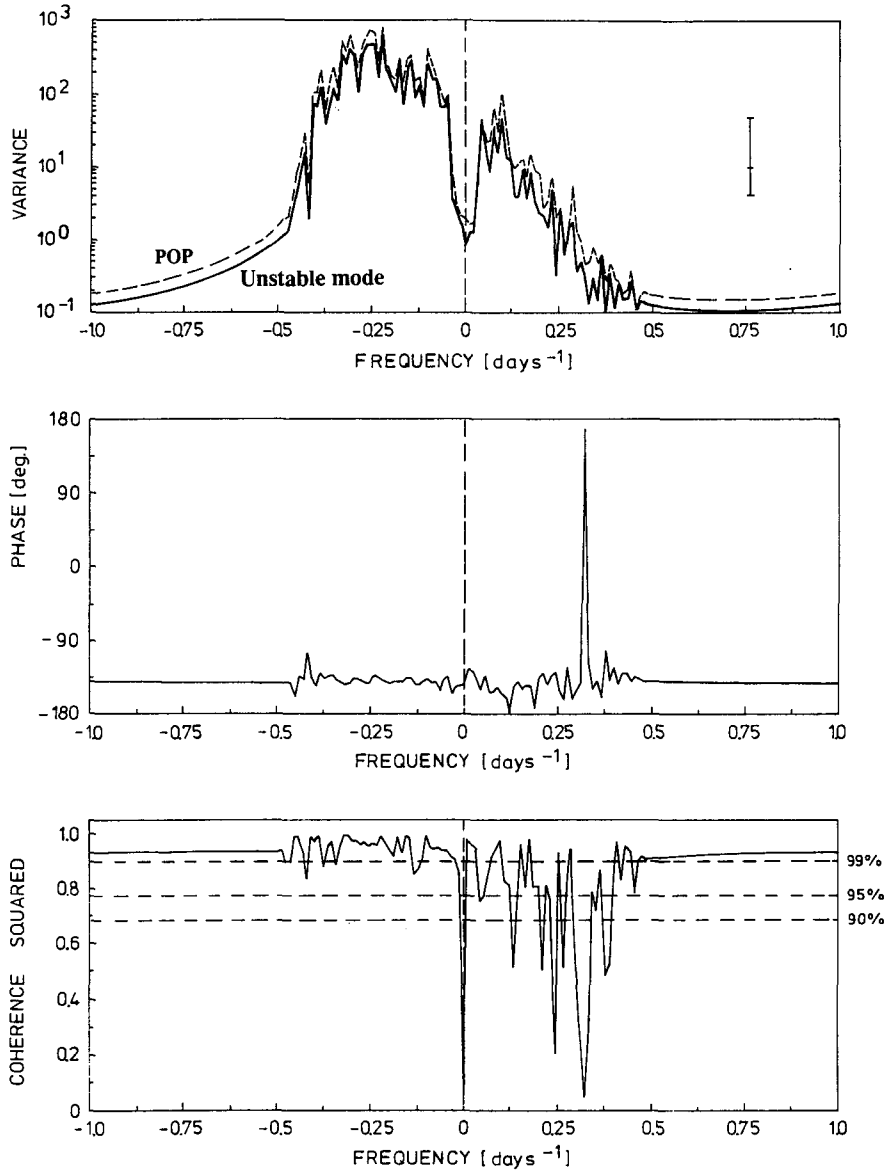

FIG. 5. Baroclinic waves: Complex cross-spectral analysis between the (complex) POP coefficient time series and the (complex) coefficient time series of the unstable normal mode. The vertical dashed line marks zero frequency. Each absolute frequency contributes two components to the spectral decomposition of a complex time series: one describing a component of the time series, which rotates clockwise in the (complex) z^r/z^i plane at this (absolute) frequency, and one describing a component, which rotates anticlockwise at this same frequency. The notation here is that the negative (positive) part of the frequency axis corresponds to clockwise (anticlockwise) rotation. The phase spectrum specifies the phase offset between the two series during rotation in the z^r/z^i plane. The horizontal dashed lines in the coherence plot denote the confidence limits for the given percentage values testing the null hypothesis of zero coherency.

regularly, and they have a torus-shaped distribution in the phase space (Fig. 7a).

The second mode, on the other hand, is significant only for the surface parameters surface wind and SST (left and middle panel in Fig. 6b). It describes an eastward propagation of the surface wind signal from the Indian Ocean into the Pacific Ocean, and an almost standing feature for the SST. The POP coefficient time series oscillate, sometimes regularly, and the occurrence of El Niño and La Niña events is closely related to the oscillatory intervals. When the SO is quiet, the POP coefficients are small and noisy [see Fig. 5 in Xu (1992)]. The distribution of the POP coefficients in the phase space (Fig. 7b) is almost bivariate normal

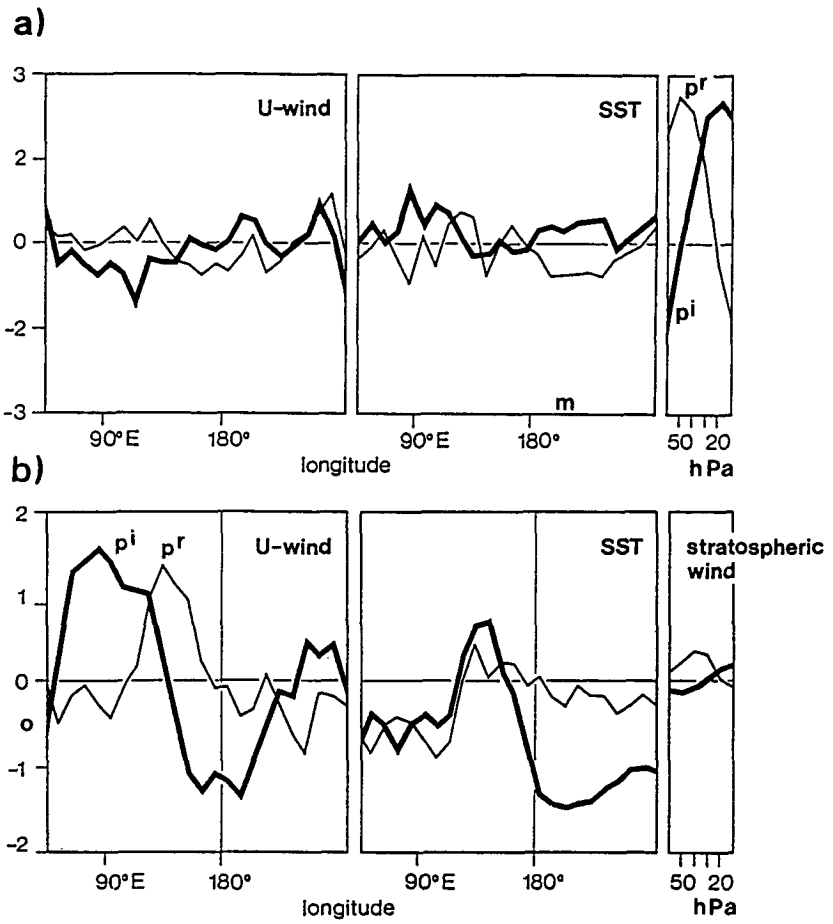

FIG. 6. QBO and SO: POP $\mathbf{p}^r$ and $\mathbf{p}^i$ from a POP analysis for a combined dataset including the stratospheric zonal wind (right panel), surface zonal wind (left panel), and SST anomalies (middle panel). The thin line is the real part $\mathbf{p}^r$ of the POP and the thick line the imaginary part $\mathbf{p}^i$. The POPs tend to appear in sequences $\cdots \rightarrow \mathbf{p}^r \rightarrow -\mathbf{p}^i \rightarrow -\mathbf{p}^r \rightarrow \mathbf{p}^i \rightarrow \mathbf{p}^r \rightarrow \cdots$; dimensionless units. Mode representing (a) the (QBO) and (b) (SO). (From Xu 1992.)

(the patterns visible in the scatter reflect serial correlation in the data).

The two POPs of the combined datasets represent the QBO and the SO. The correlations between the POP coefficient time series of the two modes are negligible around the period of the two modes. Thus, the two modes are identified as being, to first-order approximation, statistically independent.

c. *The Madden and Julian oscillation—sensitivity to analysis time interval and analysis area*

The Madden and Julian oscillation (MJO), or the tropical 30–60 day oscillation, is particularly well reflected in equatorial tropospheric velocity potential. Five years of daily NMC analyses of 200-hPa velocity potential from May 1984 to April 1989 were available. From these data the annual cycle was removed.

A total of six POP analyses was done for different subsets of the complete dataset (von Storch and Xu 1990). Two analyses, named "A" and "B", use data along the entire equator: "A" uses data from a two-year subset and in "B" the whole five-year dataset is analyzed. In the four other experiments, named "C"–"F", five years of data are considered as in "B"; in space, however, the input data for the POP analysis are restricted to equatorial 90° sectors, from 0°–90°E, 90°E–180°, etc.

In all six analyses one physically significant complex POP is identified. To make the comparisons easier, the POPs are rotated so that the $\mathbf{p}^r$ patterns optimally fit the "A"–$\mathbf{p}^r$ pattern. This operation is not in conflict with the POP concept since pairs of POPs are defined as complex eigenvectors, which may be multiplied by any complex number.

The POP obtained in the "A" analysis has a period of $T = 44$ days and an e-folding time of 13 days (about 30% of T). The squared coherency of the POP coefficients is larger than 68% on timescales between 20

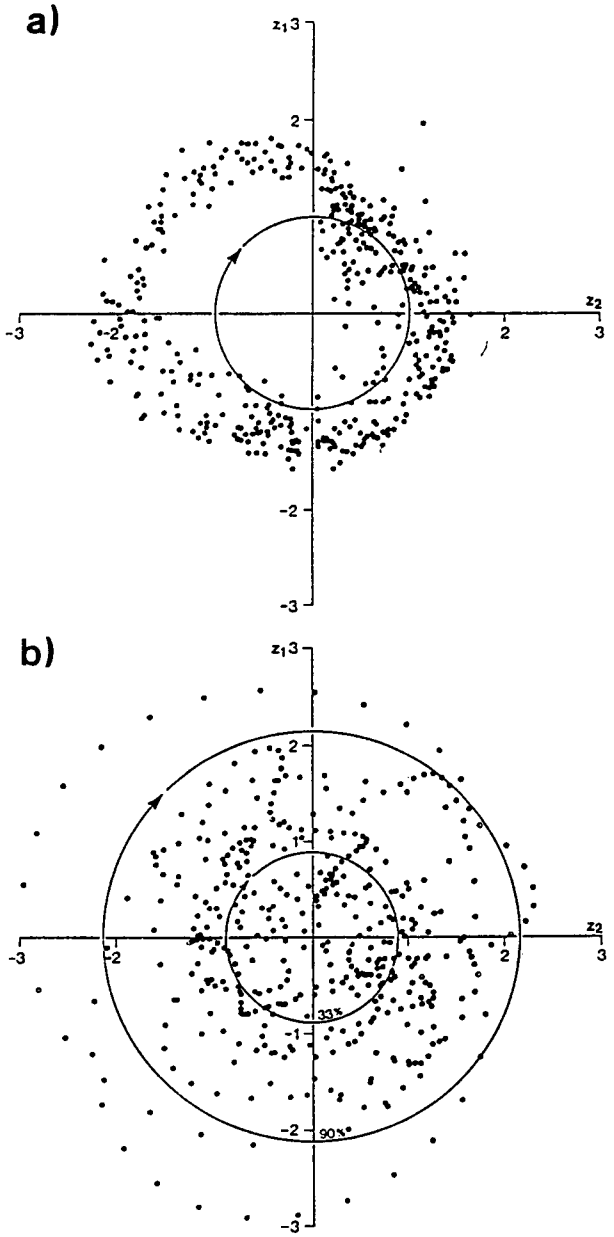

FIG. 7. QBO and SO: Distributions of the complex POP coefficients connected with the patterns shown in Fig. 6. The coefficients of (a) the QBO mode and (b) the SO mode. (From Xu 1992.)

and 50 days with a maximum value of 96% at 50 days. The patterns $\mathbf{p}^r$ and $\mathbf{p}^i$ are shown as solid lines in Fig. 8a. They are zonal wavenumber 1 type patterns with one minimum and one maximum. The two patterns are about 90° out of phase, indicating an eastward migration of the signal. The speed of the eastward movement of the minimum (and of the maximum) changes during a POP cycle.

The extension of the time interval, in the "B" analysis, from the 2-year subinterval to the full five year dataset is not connected with noteworthy changes of the characteristic numbers. The "B" patterns shown in Fig. 8a (dashed lines) are almost identical to the "A" patterns.

In the set of "C"–"F" analyses adjacent 90° sectors are considered. The 90° sector patterns closely resemble the full 360° patterns (Fig. 8b). That the $\mathbf{p}^r$ patterns fit better than the $\mathbf{p}^i$ patterns is due to the aforementioned rotation of the POPs.

The characteristic numbers deviate from the "A" and "B" results. The *e*-folding times in the 90° sectors are considerably smaller than in "A" and "B". This difference is reasonable: the POPs describe a global, traveling feature that will be traced for a longer time in the 360° circle than in the 90° sectors. Interestingly, the damping time in the Eastern Hemisphere (seven days) is about twice that in the Western Hemisphere (four days). This finding is consistent with the observation that the 30–60-day oscillation is markedly stronger in the Eastern Hemisphere. The differences in the periods in the four 90° sectors is consistent with the variable longitudinal phase speed of the MJO. In

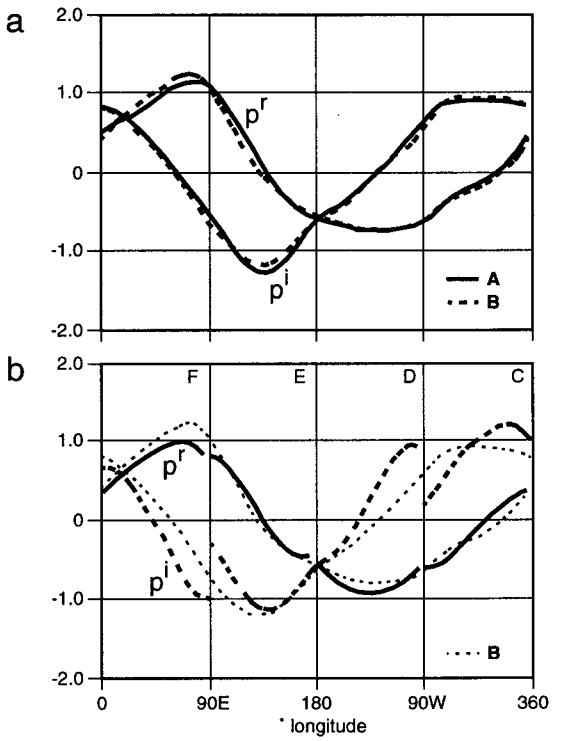

FIG. 8. MJO: POPs $\mathbf{p}^r$ and $\mathbf{p}^i$ of equatorial 200-mb velocity potential. The POPs tend to appear in sequences $\cdots \rightarrow \mathbf{p}^r \rightarrow -\mathbf{p}^i \rightarrow -\mathbf{p}^r \rightarrow \mathbf{p}^i \rightarrow \mathbf{p}^r \rightarrow \cdots$; dimensionless units. (a) Analysis of equatorial data from a 2-year subset of data (analysis "A"; solid line) and from the complete 5-year dataset (analysis "B"; dashed line). (b) The "C"–"F" analyses for 90° sectors along the equator (0°–90°E, 90°E–180°, 180°–90°W, and 90°W–0°). The vector $\mathbf{p}^r$ is given as a solid line and $\mathbf{p}^2$ as a dashed line. The full 360° analysis patterns shown in (a) are indicated with dots for comparison. The POPs have been rotated so that $\mathbf{p}^r$ fits the "A" – $\mathbf{p}^r$. (From von Storch and Xu 1990.)

the 90°E–180° sector, the MJO is slowest and $T = 62$ days. In the 180°–90°W sector, the propagation is fastest and the period is minimum; namely, $T = 33$ days. The "C"–"F" average T is 45 days, almost identical to T of the 360° analyses "A" and "B".

We conclude that the POP technique is able to infer a signal even from a space–time subset of data.

4. POPs as a predictive tool

a. *The POP forecast technique*

The POP technique is naturally suited for predictions (Xu and von Storch 1990; Xu 1990; von Storch and Xu 1990; Penland and Ghil 1993; Tang 1994; Tang et al. 1994; Xue et al. 1994; Wu et al. 1994) because of the forecast equation (11) for the POP coefficients, namely,

$$z(t+1) = \rho \exp^{-i(2\pi/T)} z(t) \qquad (28)$$

with the period $T = 2\pi/\eta = 2\pi/\tan^{-1}(\mathrm{Im}\lambda/\mathrm{Re}\lambda)$ and $\rho = |\lambda|$. Equation (28) describes the damped persistence of a trajectory in the complex plane (Fig. 1). Thus, in the framework of the POP prediction, it is only necessary to identify the location in the complex state space of the system at a given time to predict future locations. For a limited time this prediction might be useful, but at longer lead times the built-in linearity of the POP analysis as well as the unpredictable noise will result in a deterioration of the forecast skill.

Equation (28) always forecasts a decay of the amplitude (because of $\rho < 1$). However, for a stationary time series the probability of a decay at any given time equals the probability of an intensification, namely 50%. Therefore, we respecify ρ in (28) as $\rho = 1$ so that the forecast becomes amplitudewise a persistence forecast. Thus, we may expect a nontrivial forecast only for a regularly changing phase. However, a prediction of phase is valuable even if the amplitude is not well predicted.

In principle, one could make forecasts with all POPs derived in a POP analysis by applying (30) to each POP coefficient separately. It is our experience, though, that a useful forecast is obtained only for those POPs that represent a "mode" of the considered system, such as ENSO, the MJO, or the QBO. This experience is supported by the recent study of Tang et al. (1994), who made a POP analysis of ENSO-related data and Arctic sea ice data. They were successful in identifying a well-predictable ENSO mode, whereas the modes that came out of the POP analysis of Arctic data and could not be understood physically did not offer any useful predictive skill.

Because of the often noisy character of the analyzed variable it is not sufficient to estimate the POP coefficient for a certain date and to use this as initial value. Instead, some initialization is necessary. In the "time filtering" initialization (Xu and von Storch 1990) a one-sided digital filter is used to suppress variance on short timescales. In the time-averaging initialization (von Storch and Xu 1990) the POP coefficients are derived for the last few times. Then, a one-time-step POP forecast is made with the POP coefficients analyzed at time -1, a two-time-step forecast is made with the data of time -2, etc. A weighted average of the various forecasts and of the analysis at time 0 is used as the initial value. More weight is given to the recent information and less to the older information.

POP coefficients that are small and move irregularly in the two-dimensional phase space indicate that the considered process is not active and that the entire system is in a "quiet phase." In that case it would be reasonable not to rely on the formal POP forecast. Instead, the adequate POP forecast is that the system will stay in the quiet phase.

To measure the quality of the POP forecasts, two measures of skill are used: the correlation skill score $\mathcal{S}(\tau)$ and the rms skill score $\mathcal{R}(\tau)$:

$$\mathcal{S}(\tau) = \frac{\langle \hat{z}_\tau^*(t) \cdot z(t) \rangle}{\sqrt{\langle |\hat{z}_\tau(t)|^2 \rangle \cdot \langle |z(t)|^2 \rangle}} \qquad (29)$$

$$\mathcal{R}(\tau) = \sqrt{\langle |\hat{z}_\tau(t) - z(t)|^2 \rangle}, \qquad (30)$$

where $\hat{z}_\tau(t)$ denotes the (complex) forecast issued at time $t - \tau$ for τ time steps in advance, $z(t)$ is the (complex) verifying quantity, and the angle brackets indicate ensemble averages.

The correlation skill score $\mathcal{S}(\tau)$, being insensitive to amplitude errors, is an indicator of phase errors only. With respect to the amplitude the POP forecast is a persistence forecast. Therefore, $\mathcal{S}(\tau)$ is an adequate skill score of the POP method; $\mathcal{R}(\tau)$ is sensitive to both phase and amplitude errors. It may be anticipated, therefore, that the POP forecast appears less successful if measured in terms of rms error.

To evaluate the merits of the POP forecast, its skill is compared with an even simpler forecast: the persistence forecast. Persistence is a fair choice as a competitor because the POP forecast and the persistence may be seen next to each other in an hierarchy of forecast schemes of increasing complexity.

b. *Example: the Madden and Julian oscillation*

In von Storch and Xu (1990) and von Storch and Baumhefner (1991), the skill of the POP technique in predicting the MJO (see section 3c) was examined. In this case, the time-averaging initialization, exploiting the information from day 0 through day -4, was used to estimate the initial value. The POP amplitude $|z|$ is predicted by persistence, that is, $\rho = 1$ in (28).

Individual forecasts are presented in the form of a "dial" diagram showing the evolutions of the POP coefficients derived from the analysis data before and after the forecast date and the forecast itself. Two cases are

considered: 30 January 1985 and 1 December 1988. For these two dates not only POP forecasts are available but also forecasts made with the NCAR Climate Community Model (CCM).

Figure 9a shows the predicted and analyzed evolution for 30 days beginning on 30 January 1985. The MJO developed regularly, with a clockwise rotation in the plane spanned by the real and imaginary part of the POP coefficients, until about 26 February. After that day the MJO moved backwards. Both forecasts, the POP forecast as well as the NCAR CCM forecast, are skillful in predicting the regular evolution in the first 25 days, but fail with the phase reversal on 25 February.

Figure 9b shows the less successful forecast of 1 December 1988. The POP coefficient z of the MJO was small on day 0 and remained so. In the velocity potential field a well-defined wavenumber 1 pattern was not present (not shown). Therefore, the failure of both forecasts is not unexpected.

The correlation skill score $\mathcal{S}(\tau)$ and the rms error skill score $\mathcal{R}(\tau)$, derived from a large ensemble of forecast experiments, are shown in Fig. 10 for the POP scheme and for persistence. During the first two days the persistence is more skillful than the POP forecast, but after this time the persistence forecast rapidly loses its skill. For persistence, $\mathcal{S}(\tau)$ has a minimum after about 20 days, indicating the 30–60 day oscillatory behavior of the MJO, and $\mathcal{R}(\tau)$ reaches its saturation level. For the POP forecast, $\mathcal{S}(\tau)$ slowly decreases with time, crossing the critical 0.5 level after about 9 days. The increase of $\mathcal{R}(\tau)$ is considerably slower than in the case of the persistence. Even after 24 days the saturation level is not yet reached.

It was also analyzed whether the skill of the POP forecast of the MJO would depend on factors known at the time of the forecast [Fig. 11 in von Storch and Xu (1990) and Fig. 6 in von Storch and Baumhefner (1991)]. It turned out that the skill was insensitive to the initial phase. The amplitude, however, had a marked impact: the larger the signal at the initial time, the longer a skillfull prediction by the POP method. Such a property is obviously favorable since it allows, at least in principle, the prediction of the prediction skill. It turned out that a numerical forecast model predicted the MJO signal with some skill for about 6 days in advance, when the initial state had a large POP coefficient. Initial states with small initial POP coefficients, on the other hand, gave poor predictions of the MJO signal: the critical 0.50 correlation skill level was passed already within 1 day [Fig. 16 in von Storch and Baumhefner (1991)].

5. Cyclostationary POP analysis

The POP analysis that was described in section 2 operates on the assumption of stationary time series.

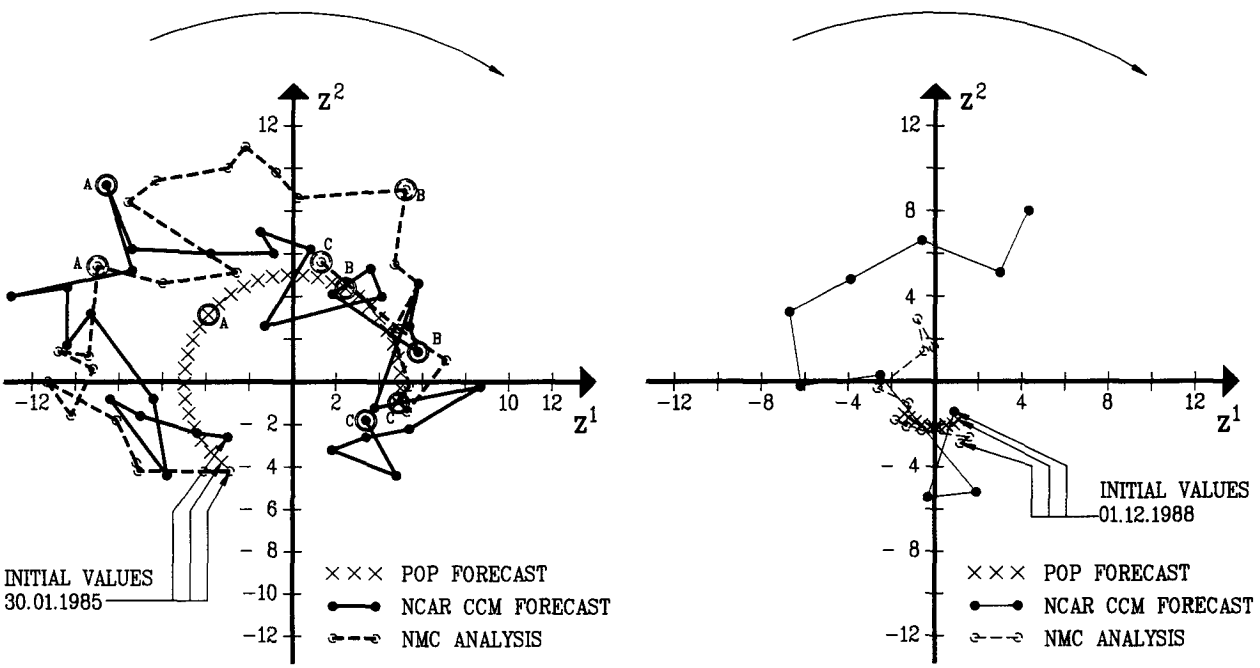

FIG. 9. MJO: Forecasts of the POP coefficient z for (a) 30 January 1985 and (b) for 1 December 1988. The forecasts are presented in the two-dimensional POP-coefficient plane with the x axis representing the z^r coefficient, and the y axis the z^i coefficient. The POP forecast model (28) implies a clockwise rotation of the trajectory. The dashed line that connects the open circles represents the observed evolution, the continuous line that connects the solid circles represents a forecast prepared with the NCAR CCM, and the POP forecast is given by the crosses. The big labeled circles in (a) indicate the following dates in 1985: A: 10 Feb, B: 20 Feb, C: 1 Mar. (von Storch and Baumhefner 1991.)

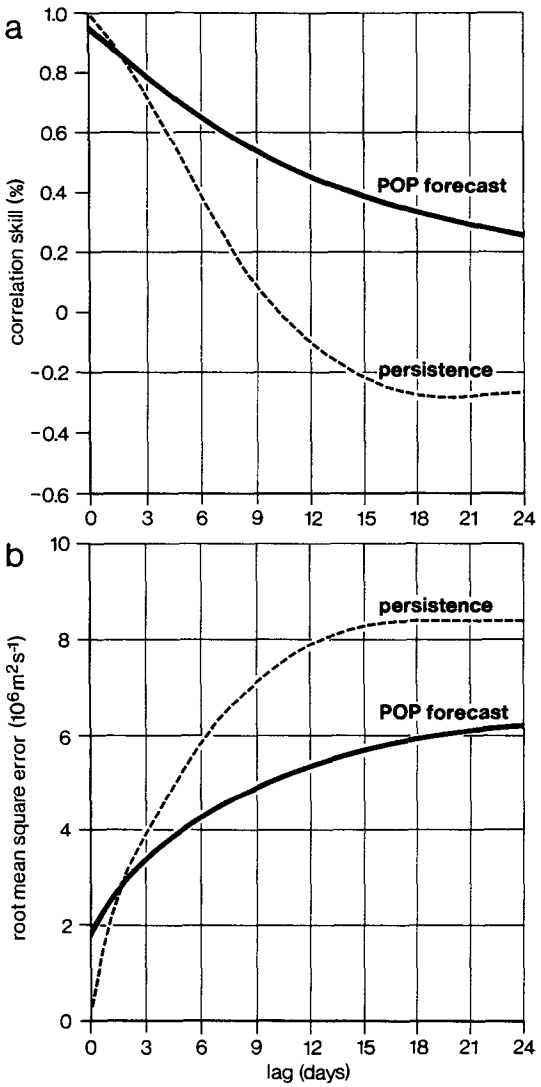

FIG. 10. MJO: Skill scores of the POP forecast (solid) and of persistence (dashed) in predicting the MJO. (a) Correlation skill (29), $\mathcal{S}(\tau)$: a 100% indicates perfect skill, a 0 a useless forecast. (b) Rms skill (30), $\mathcal{R}(\tau)$. (von Storch and Xu 1990.)

In many practical situations, however, the time series are not stationary but *cyclostationary;* that is, the first and second moments depend on an external cycle. This cycle is often the annual cycle or the diurnal cycle. In this section, we present a generalization of the conventional POP analysis that explicitly takes into account this nonstationarity.

The cyclostationary POP analysis has been suggested first by Hasselmann in a unpublished manuscript in 1985. In 1989/1990, two groups, namely, Maria Ortiz and her colleagues at the University of Alcala in Spain and Benno Blumenthal from Lamont, showed independently how to practically implement the cyclostationary POP analysis; only Blumenthal published his results (Blumenthal 1991).

a. Definition

Time is given by a pair of integers (t, τ) with t counting the cycles (e.g., annual cycle) and τ counting the seasonal date (e.g., month), that is, the time steps within a cycle with $\tau = 1, \ldots, n$. It is $(t, n+1) = (t+1, 1)$ or, generally, $(t, \tau + n) = (t + 1, \tau)$. Then the cyclostationary process may be written as

$$\mathbf{x}(t, \tau + 1) = \mathcal{A}(\tau) \cdot \mathbf{x}(t, \tau) + \text{noise} \quad (31)$$

with $\mathbf{x}(t, \tau + n) = \mathbf{x}(t + 1, \tau)$ and $\mathcal{A}(\tau + n) = \mathcal{A}(\tau)$. Applying (31) consecutively n times, we find with

$$\mathcal{B}(\tau) = \mathcal{A}(\tau + n - 1)\mathcal{A}(\tau + n - 2) \cdots \mathcal{A}(\tau + 1)\mathcal{A}(\tau) \quad (32)$$

that

$$\mathbf{x}(t + 1, \tau) = \mathcal{B}(\tau)\mathbf{x}(t, \tau) + \text{noise}. \quad (33)$$

Because of the imposed periodicity there are n models of the form (33). To each of these models a conventional POP analysis can be applied. In this way eigenvectors $\mathbf{p}^\tau$ and eigenvalues λ^τ are obtained:

$$\mathcal{B}(\tau)\mathbf{p}^\tau = \lambda^\tau \mathbf{p}^\tau \quad (34)$$

with $[\mathbf{p}^\tau]^{T*} \cdot \mathbf{p}^\tau = 1$. The eigenvalues λ^τ are the same for different $\mathcal{B}(\tau)$ models:

$$\begin{aligned} &\mathcal{B}(\tau)\mathbf{p}^\tau = \lambda^\tau \mathbf{p}^\tau \\ \Leftrightarrow\ &\mathcal{A}(\tau + n)\mathcal{B}(\tau)\mathbf{p}^\tau = \lambda^\tau \mathcal{A}(\tau + n)\mathbf{p}^\tau \\ \Leftrightarrow\ &\mathcal{B}(\tau + 1)[\mathcal{A}(\tau)\mathbf{p}^\tau] = \lambda^\tau [\mathcal{A}(\tau)\mathbf{p}^\tau]. \end{aligned} \quad (35)$$

Thus, $\mathcal{B}(\tau + 1)$ and $\mathcal{B}(\tau)$ share the same eigenvalues, and $\mathcal{A}(\tau)\mathbf{p}^\tau$ is an eigenvector of $\mathcal{B}(\tau + 1)$ if $\mathbf{p}^\tau$ is an eigenvector of $\mathcal{B}(\tau)$. Eigenvectors may be multiplied with any complex number $c = r_\tau^{-1} \exp i\phi_\tau$:

$$\mathbf{p}^{\tau+1} = (r_\tau^{-1} \exp i\phi_\tau)\mathcal{A}(\tau)\mathbf{p}^\tau. \quad (36)$$

The modulus $|r_\tau^{-1} \cdot \exp i\phi_\tau| = r_\tau^{-1}$ is chosen such that $[\mathbf{p}^\tau]^{T*}\mathbf{p}^\tau = 1$. If, for a certain τ, the normalization condition $(\mathbf{p}^\tau)^{T*}\mathbf{p}^\tau = 1$ is fulfilled, then $[\mathbf{p}^{\tau+1}]^{T*}\mathbf{p}^{\tau+1} = 1$ if

$$r_\tau = \|\mathcal{A}(\tau)\mathbf{p}^\tau\|. \quad (37)$$

The angle ϕ_τ is determined so that the periodicity condition $\mathbf{p}^{\tau+n} = \mathbf{p}^\tau$ is satisfied:

$$\phi_\tau = \eta/n \quad \text{for all } \tau \quad (38)$$

with $\lambda = \rho \exp(-i\eta)$. The relations (37) and (38) are reasonable: Within one cycle, the POP is damped by the factor ρ and rotated by an angle $-\eta$. Thus, to ensure $\mathbf{p}^{\tau+n} = \mathbf{p}^\tau$, at each time step the pattern is amplified by r_τ and rotated backwards by η/n. For the POP coefficients $z(t)$ a time evolution equation similar to (11) holds:

$$z(t, \tau + 1) = r_\tau \exp(-i\eta/n)z(t, \tau) + \text{noise}. \quad (39)$$

Repeated application of (39) yields, not unexpectedly, the conventional POP model result (11):

$$z(t+1,\tau) = \left(\prod_{k=0}^{n-1} r_{\tau+k}\right)\exp(-i\eta)z(t,\tau) + \text{noise}$$

$$= \lambda z(t,\tau) + \text{noise} \qquad (40)$$

so that $\rho = \prod_{k=0}^{n-1} r_{\tau+k}$.

The time coefficients at a given time t may be obtained by projecting the full field $\mathbf{x}(t, \tau)$ onto the respective adjoint $[\mathbf{p}^A]^\tau$ or by using a least-square approximation (17), (18). The adjoint patterns $[\mathbf{p}^A]^\tau$ and $[\mathbf{p}^A]^{\tau+1}$ are related to each other through a simple formula, similar to (36):

$$[\mathbf{p}^A]^\tau = r_\tau^{-1} \cdot \exp(i\phi) \cdot \mathcal{A}(\tau)^T [\mathbf{p}^A]^{\tau+1}. \qquad (41)$$

A straightforward estimation of the $\mathcal{A}(\tau)$ is to use (10) for each $\tau = 1, \cdots, n$:

$$\mathcal{A}(\tau) = \mathcal{X}_{1,\tau}\mathcal{X}_{0,\tau}^{-1}. \qquad (42)$$

b. Example

The Southern Oscillation is known to be phase locked to the annual cycle (Rasmusson and Carpenter 1982). Thus, the time series of surface wind and SST along the equator from 50°E to 80°W (already used in section 3b) are good candidates for a cyclostationary POP analysis. Monthly anomalies are analyzed; thus, $n = 12$. The data are time filtered to suppress the month-to-month variability; all variability on timescales longer than 12 mo is retained. Parallel to the cyclostationary POP analysis, a conventional POP analysis has been performed.

In both POP analyses one dominant POP mode is found. The periods of $T = 31$ mo (cyclostationary analysis) and $T = 34$ mo (stationary analysis) are comparable. The mode identified in the stationary analysis is consistent with the $T = 28$ mo mode found in section 3b (Figs. 6b and 7b).

The damping rate r_τ exhibits a marked nonsinusoidal annual cycle (Fig. 11). Amplification takes place from April to September with a maximum in June. The process is damped from October to March with a minimum in February. Thus, the time lag between the minimum and the maximum is only 4 mo, whereas the lag between maximum and minimum is 8 mo. The annually averaged damping rate is almost identical with the damping rate obtained in the stationary analysis (Fig. 11).

The annual r_τ cycle is consistent with the annual cycle of the persistence of various SO indices (Wright 1985). In a PIP analysis Weese (in von Storch et al. 1990) fitted a sinusoidal damping rate to the same data that we used. He also found an amplification in northern summer and a damping in winter. His annual range, however, was much smaller (~0.08) than is the case here (~0.25).

The *zonal wind* patterns (Fig. 12a) show some eastward progression with the annual cycle. The real component is strongest during the first half of the year, whereas the imaginary component is strongest during the second half.

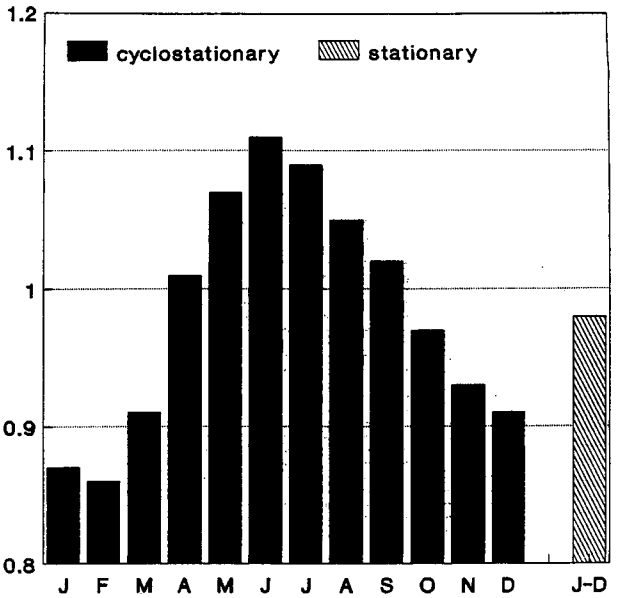

FIG. 11. ENSO: Damping rates obtained in the stationary POP analysis and in the cyclostationary POP analysis of the Southern Oscillation (in terms of equatorial zonal surface wind and SST). For the stationary analysis, one damping rate representing the average damping from one month to the next is shown. For the cyclostationary analysis, a separate damping rate is obtained for each month.

The *SST* real pattern (Fig. 12b) has a notable amplitude in the Indian Ocean and some significant structure in the East Pacific, but only in northern winter. The imaginary component has an amplitude ≥ 0.2 throughout the year in the East Pacific, with a maximum in northern fall. At the same time a significant amplitude with opposite sign is identified in the West Pacific.

The annual average of the cyclostationary modes is similar to the pattern of the stationary POP analysis (Fig. 6a).

Note that the wind data and the SST data have both been normalized to variance 1 prior to the POP analysis. To transform the patterns to meaningful physical units, the wind patterns (Fig. 12a) have to be multiplied with 0.45 and with the standard deviations of the POP coefficients (Fig. 14). Similarly, typical amplitudes of SST are obtained by multiplication of the patterns by 0.60 and the standard deviation of the POP coefficients.

If the considered state at some time is represented by our cyclostationary POP, then it may be represented by $\mathbf{P}(0, \tau) = 2\,\mathrm{Re}[z(0, \tau) \cdot \mathbf{p}^\tau]$. Its future state at time t is then given by

$$\mathbf{P}(0, t+\tau) = 2\,\mathrm{Re}\left(\prod_{\delta=1}^{t} [r_{\tau+\delta}\exp(i\eta/n)]z(0,\tau)\mathbf{p}^{\tau+t}\right)$$

$$+ \text{noise}. \qquad (43)$$

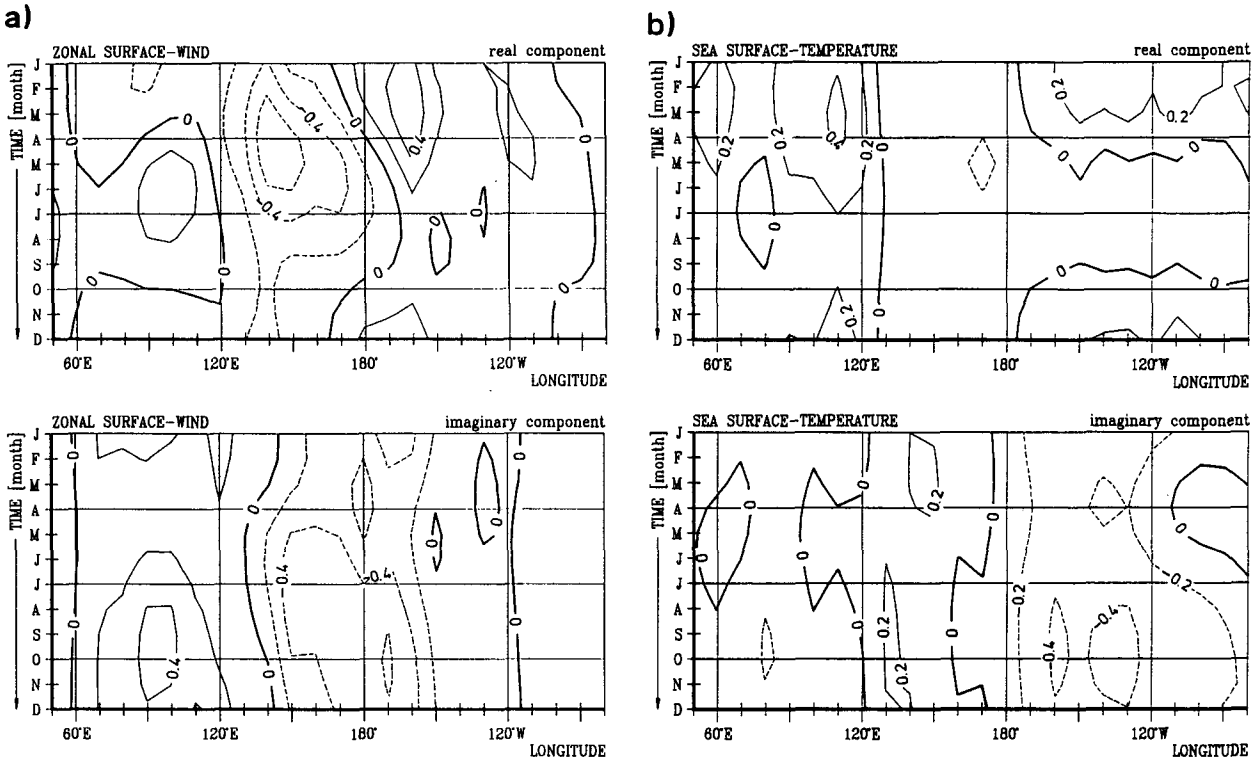

FIG. 12. ENSO: Cyclostationary POPs of the combined normalized zonal wind–SST dataset. The horizontal axis represents the longitude along the equator, and the vertical axis denotes the annual cycle. (a) Real and imaginary component of the zonal wind pattern. (b) Real and imaginary component of the SST pattern.

By neglecting the noise term, it is possible to construct typical evolutions that are connected with certain initial states. In Fig. 13, these evolutions are shown for two initial states in January and July. The initial states are either $\mathrm{Re}(\mathbf{p}^r)$ or $\mathrm{Im}(\mathbf{p}^r)$. The initial states $\mathrm{Re}(\mathbf{p}^{\mathrm{Jul}})$ and $\mathrm{Im}(\mathbf{p}^{\mathrm{Jan}})$ are not connected with the evolution of noteworthy anomalies in the zonal wind or in the SST (Fig. 13). Instead, the initially existing anomalies are quickly damped. However, the other two initial states, $\mathrm{Im}(\mathbf{p}^{\mathrm{Jul}})$ and $\mathrm{Re}(\mathbf{p}^{\mathrm{Jan}})$, are precursors for the evolution of El Niño and La Niña events (Fig. 13).

The variances of the POP coefficients have a marked annual cycle (Fig. 14). The annual average is about 5. The real component has a minimum of only 2 in May and a maximum of 9 in November. The imaginary component has a minimum of 4 in March and a maximum of 8 in September.

6. Complex POP analysis

a. *Definition of Complex POPs*

By definition, a *standing oscillation* can be described by a single pattern together with an amplitude. Thus, the sequence (7) requires $\mathbf{p}^r = \alpha \mathbf{p}^i$ with some real number α for a standing oscillation. Such a relationship implies that the corresponding eigenvalue is *real* and the spectrum (21) is red, so that the considered process is not oscillatory but a damped system. Thus, the linear system (1) is not able to model a standing oscillation. The background of this is that the description of an oscillating process requires not only the state of the system but also its tendency, or its *momentum*. From Hamiltonian mechanics we know that the momentum describes a process that evolves in quadrature to the original process. As "process and conjugate process," they perform a perfect cycle in a two-dimensional phase space. For traveling modes this momentum is hidden in the spatial pattern of the system. In the case of standing oscillations, however, the momentum is not determined by the simultaneous pattern—in fact, this pattern is constant for a standing oscillation.

The idea behind the Complex POP (CPOP) analysis is to construct a momentum time series $\dot{\mathbf{x}}(t)$. In contrast to continuous processes where the definition of "momentum" is straightforward via the time derivation, there is no unique definition of momentum for discrete processes. One reasonable definition is obtained by means of the *Hilbert transform* (Wallace and Dickinson 1972; Barnett and Preisendorfer 1981): If $x(t)$ is a real time series with Fourier decomposition

$$\mathbf{x}(t) = \sum_{\omega} \zeta(\omega) \exp(i\omega t), \qquad (44)$$

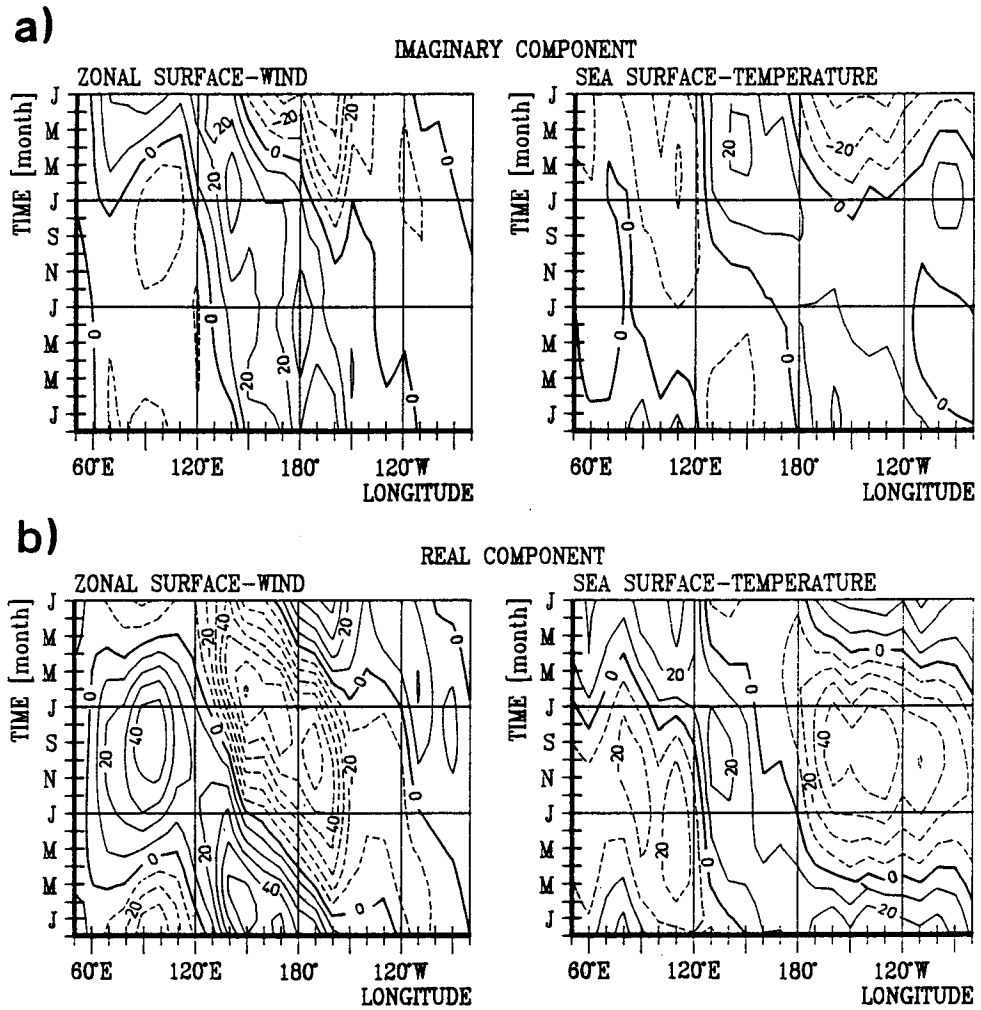

FIG. 13. ENSO: Evolution of SST and zonal wind if different initial states are prescribed. The horizontal axes represent the longitudinal position, and the vertical axes represent time in 24-month intervals, increasing in downward direction. (a) Imaginary component and (b) real component of POP is used as initial state in

the Hilbert transform of $\mathbf{x}$ is

$$\dot{\mathbf{x}}(t) = \sum_{\omega} \theta(\omega) \exp i(\omega t + \pi/2), \tag{45}$$

where $\theta(\omega)$ is defined to be

$$\theta(\omega) = \begin{cases} \zeta(\omega) & \text{for} \quad \omega \leqslant \pi \\ \zeta^*(\omega) & \text{for} \quad \omega > \pi. \end{cases} \tag{46}$$

Here $\dot{\mathbf{x}}$ is identical to $\mathbf{x}(t)$ apart from a $\pi/2$ phase shift of θ taken uniformly at each frequency ω.

Complex POPs are obtained by assuming a first-order linear model (1) for the complex vector $\mathbf{w} = \mathbf{x}(t) + i \cdot \dot{\mathbf{x}}(t)$:

$$\mathbf{w}(t+1) = \mathcal{W} \cdot \mathbf{w}(t) + \text{noise}. \tag{47}$$

The complex matrix $\mathcal{W}$ is estimated from the data as in (10) by

$$\mathcal{W} = E[\mathbf{w}(t+1) \cdot \mathbf{w}^{T^*}(t)] \cdot [E[\mathbf{w}(t) \cdot \mathbf{w}^{T^*}(t)]]^{-1}. \tag{48}$$

The eigenvectors of $\mathcal{W}$ are the *CPOPs*. Since $\mathcal{W}$ is complex, the eigenvectors do not appear in conjugate complex pairs so that, different from the real or standard POPs, the number of CPOPs equals the dimension of the process (47).

To find the CPOP coefficients, we expand the *complex* state $\mathbf{w}(t)$ in terms of the CPOP basis:

$$\mathbf{w}(t) = \sum_j \gamma_j(t) \mathbf{p}_j. \tag{49}$$

At any given time t, the contribution of the CPOP $\mathbf{p}$ to the full $\mathbf{w}(t)$ is given by the complex process $\mathbf{P}(t) = \gamma(t) \cdot \mathbf{p}$, or, with $\mathbf{P} = \mathbf{P}^1 + i\mathbf{P}^2$, $\mathbf{p} = \mathbf{p}^r + i\mathbf{p}^i$ and $\gamma = \gamma^1 - i\gamma^2$:

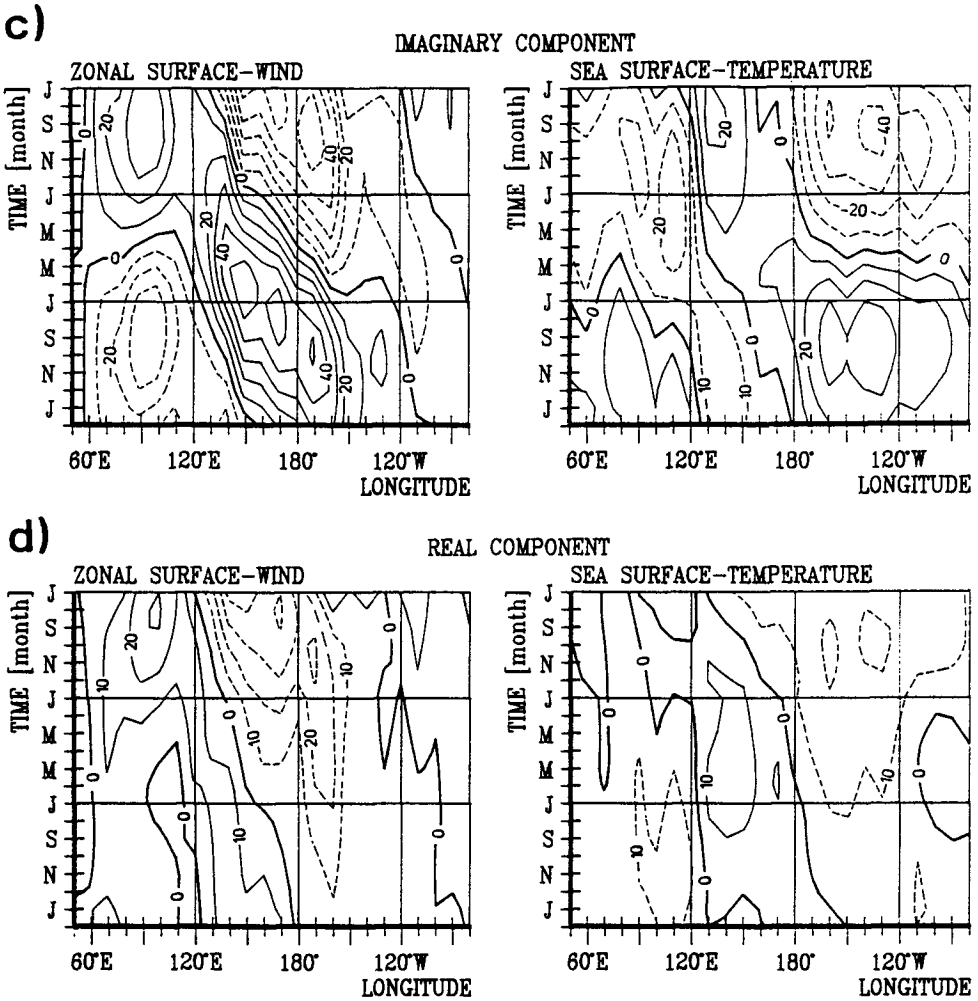

FIG. 13. (*Continued*) January; (c) imaginary component and (d) real component of POP is used as initial state in Jul.

$$\mathbf{P}^r(t) = \gamma^1(t)\mathbf{p}^r + \gamma^2(t)\mathbf{p}^i \tag{50}$$

$$\mathbf{P}^i(t) = \gamma^1(t)\mathbf{p}^i - \gamma^2(t)\mathbf{p}^r. \tag{51}$$

The real part $\mathbf{P}^r(t)$ describes the signal in the "location" x space, whereas the imaginary part $\mathbf{P}^i(t)$ describes the signal in the momentum $\dot{\mathbf{x}}$ space. Without noise the temporal evolution of the CPOP coefficient γ is given by (11) so that (50), (51) is equivalent to

$$\mathbf{P}^r(t) = \rho^t(\cos(\eta t)\mathbf{p}^r - \sin(\eta t)\mathbf{p}^i) \tag{52}$$

$$\mathbf{P}^i(t) = \rho^t(\cos(\eta t)\mathbf{p}^i + \sin(\eta t)\mathbf{p}^r) \tag{53}$$

with $\lambda = \rho \exp(-i\eta)$. Hence, the typical evolutions are

$$\overbrace{\cdots \to \mathbf{p}^r \to -\mathbf{p}^i \to -\mathbf{p}^r \to \mathbf{p}^i \to \mathbf{p}^r \to \cdots}^{\text{x-space}}$$
$$\underbrace{\cdots \to \mathbf{p}^i \to \mathbf{p}^r \to -\mathbf{p}^i \to -\mathbf{p}^r \to \mathbf{p}^i \to \cdots}_{\dot{\text{x}}\text{-space}}$$

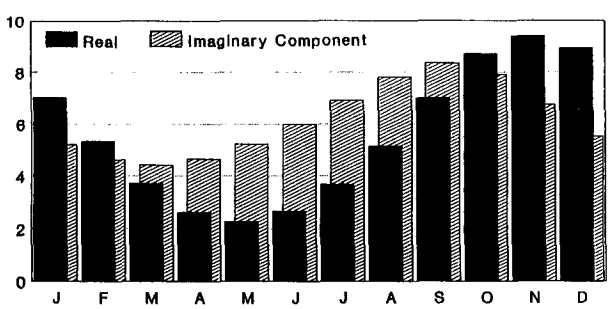

FIG. 14. ENSO: Annual cycle of the variance of the cyclostationary POP coefficients (solid: real component; hatched: imaginary component).

b. *Example: El Niño–Southern Oscillation*

To test the CPOP model and to compare with the POP model, two analyses have been performed for monthly SST anomalies along the equator from 50°E

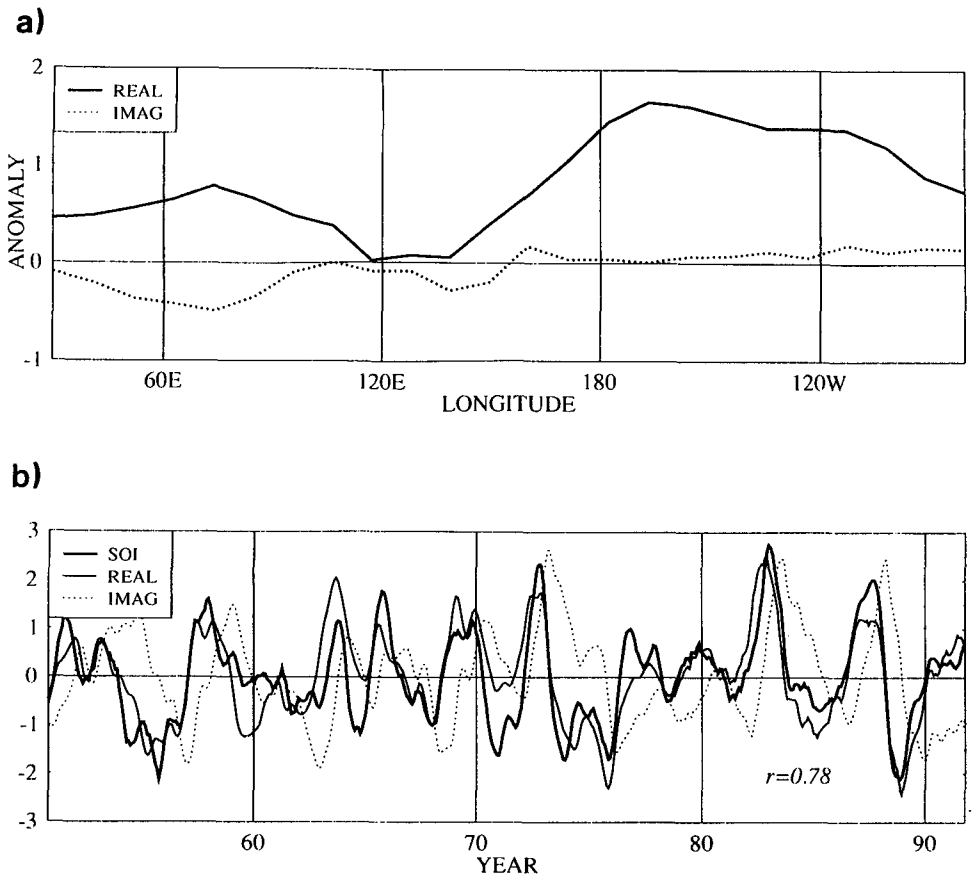

FIG. 15. ENSO: Complex POPs of equatorial SST (compare with Fig. 6b). Real and imaginary part of (a) the CPOP pattern along the equator (dimensionless unit) and (b) of the CPOP coefficient time series, together with the normalized (SST) Southern Oscillation index (unit: °C). (From Bürger 1993.)

to 80°W. These data were already used in sections 3b and 4b. The analyses have been confined to the SST because, as section 3b suggests, the expected signal is essentially standing. One dominant CPOP is resolved, explaining 30% of the data's total variance. It has a period of 39 mo and a decay time of 36 mo with highly coherent coefficients. The correlation between the CPOP coefficients and the Southern Oscillation index (SOI) is 0.78 (Fig. 15b), so that this CPOP may be identified with the Southern Oscillation. The $\mathbf{p}^r$ pattern shows a large positive temperature anomaly of up to 2°C over most of the Indian and Pacific Ocean, most strongly over the latter. The $\mathbf{p}^i$ pattern, which has only rather small values along the equator, can be viewed as the zero state of the oscillation (see Fig. 15a).

The (real) POP analysis reveals no useful patterns, thereby supporting the argument above. Only by bandpass filtering the data, retaining variations between 16 and 96 mo, can the same pattern as in the CPOP case be identified. The coefficients of the standard POP do not satisfactorily describe the process, as is demonstrated by Fig. 16: The amplitude time series for the standard POP is much more disturbed by noise than the amplitude of the CPOP. Similarly, the phase develops more smoothly for the CPOP.

The CPOP technique has also been used in forecast experiments. The CPOP forecast model is the same as that of the POP model (section 4) except for the determination of the initial state. The Hilbert transform is, by definition, a *noncausal* notion, and this undermines any prediction scheme. One solution of this problem is described by Bürger (1993). In the case of the ENSO example the correlation skill score is significantly enhanced compared to the forecast prepared by the standard POP (see Fig. 17).

For further details see Bürger (1993), a method is described of how to define a causal version of the Hilbert transform. In a way, the CPOP *prediction* works like an inversion of the CPOP *analysis:* Whereas for the analysis, one estimates the system matrix by means of the noncausal Hilbert transform; the causal Hilbert transform is estimated by means of the system matrix.

7. Associated correlation patterns

The POP coefficients can often be regarded as an *index* of some process, for example, of the Madden

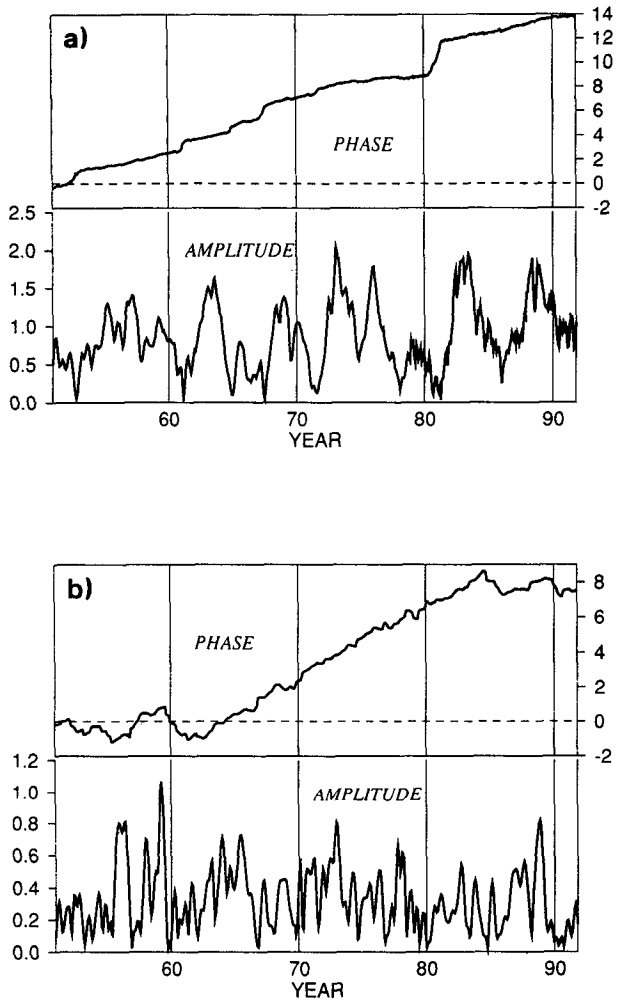

FIG. 16. Amplitude and phase of the coefficients of (a) the CPOP and (b) the real (standard) POP, both representing the ENSO process. The phase is shown without the 2π jump. (From Bürger 1993.)

and Julian oscillation or of the ENSO phenomenon. In such a case it is often desirable to be able to characterize the appearance of the process in terms of other variables. This can be achieved by means of *associated correlation patterns* (von Storch et al. 1988). Note that this concept can be applied to any uni-, bi-, or multivariate index, independently from this index being derived from a POP analysis or any other statistical approach.

For the sake of shortness, we assume that $z = (z^r + z^i)/2$ is a complex POP coefficient, and $\mathbf{v}$ any vector time series in which the signal shall be identified. Then, the associated correlation patterns are the two patterns $\mathbf{q}^r$ and $\mathbf{q}^i$ that minimize

$$\epsilon_a(\mathbf{v}) = \left\| \mathbf{v}(t) - \frac{z^r}{\sqrt{2}\sigma_r}\mathbf{q}^r - \frac{z^i}{\sqrt{2}\sigma_i}\mathbf{q}^i \right\|, \quad (54)$$

where σ_r^2 is the variance of z^r, and σ_i^2 is the variance of z^i. The interpretation of the associated correlation patterns is that, if the POPs perform cycles,

$$\cdots \rightarrow \mathbf{p}^r \rightarrow -\mathbf{p}^i \rightarrow -\mathbf{p}^r \rightarrow \mathbf{p}^i \rightarrow \mathbf{p}^r \rightarrow \cdots \quad (55)$$

the associated correlation patterns simultaneously perform the same cycle

$$\cdots \rightarrow \mathbf{q}^r \rightarrow -\mathbf{q}^i \rightarrow -\mathbf{q}^r \rightarrow \mathbf{q}^i \rightarrow \mathbf{q}^r \rightarrow \cdots. \quad (56)$$

The normalization by $\sqrt{2}\sigma_r^2$ and by $\sqrt{2}\sigma_i^2$ has been introduced to get typical patterns that occur if $z^r = 1$, $z^i = 0$, or $\mathbf{P} = \mathbf{p}^r$; or if $z^r = 0$, $z^i = 1$, or $\mathbf{P} = \mathbf{p}^i$. The solution of (54) is found by differentiating with respect to $\mathbf{q}^r$ and $\mathbf{q}^i$ and solving a 2×2 linear equation system. The spatial distribution of $\epsilon_a(\mathbf{v})$ indicates the amount of local $\mathbf{v}$ variance not represented by the POP coefficients z^r and z^i. $1 - \epsilon_a(\mathbf{v})/\mathrm{var}(\mathbf{v})$ is the rate of explained local variance, which is a good indicator of the relative importance of the POP in the $\mathbf{v}$ field.

As an example, we show associated correlation patterns for tropical outgoing longwave radiation (OLR) associated with the MJO (Figs. 18a,b). The POPs are shown in Fig. 8, and the associated patterns are derived only from the POP coefficients in southern summer so that they represent the appearance of the MJO in southern summer. The OLR signal is closely coupled to the velocity potential signal in the Eastern Hemisphere. In this area, the rate of explained day-to-day OLR variance is up to 40% (Fig. 18c).

8. Conclusions

We have demonstrated that the POP method is a powerful method to infer simultaneously the space–time

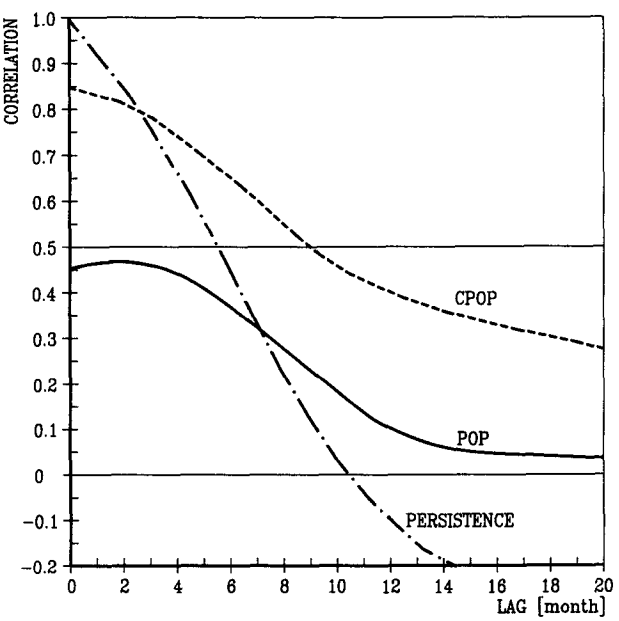

FIG. 17. Hindcast skills of the POP and CPOP predictions and of persistence. The predicted parameter is the SST index of the Southern Oscillation. (From Bürger 1993.)

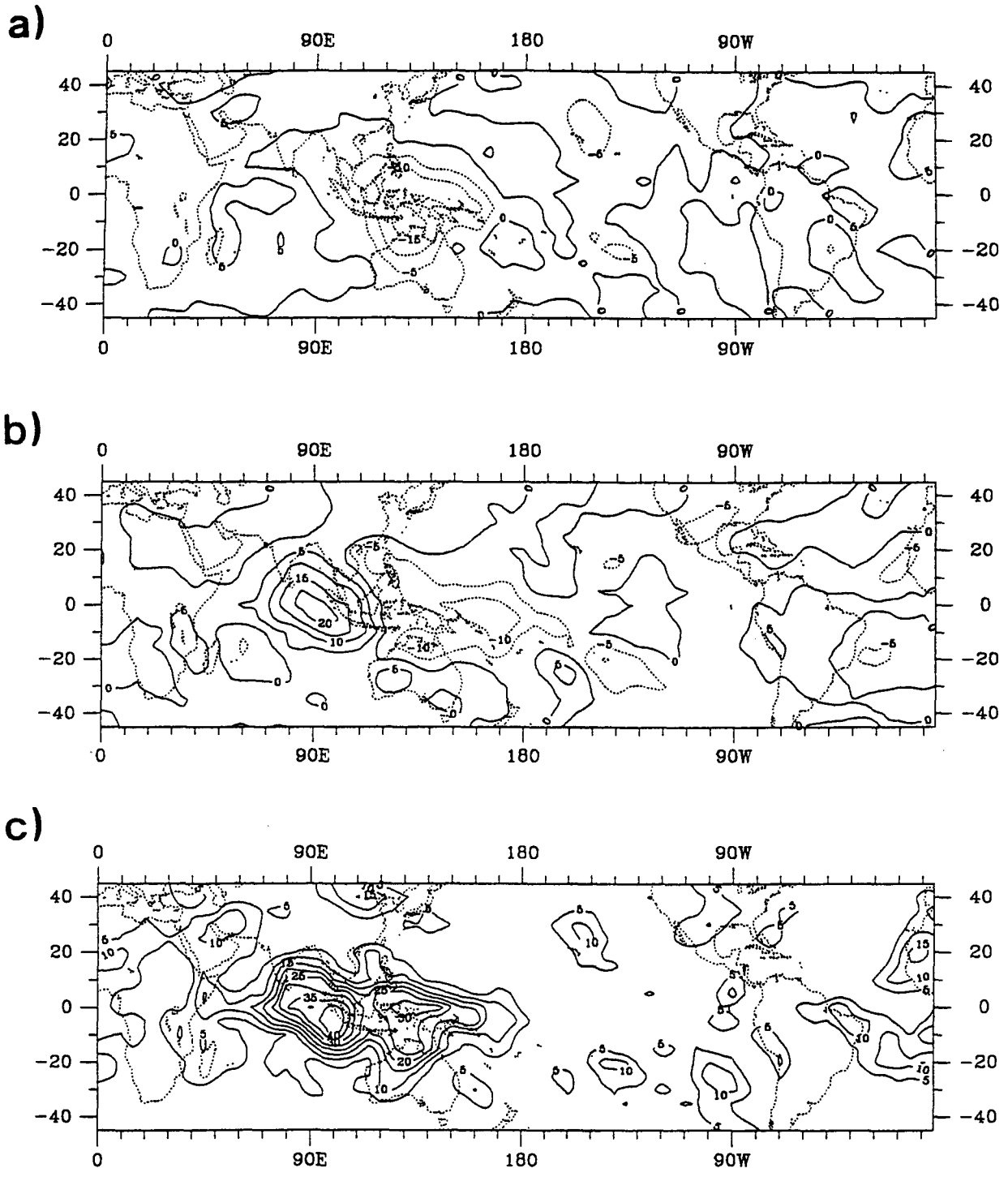

FIG. 18. Associated correlation patterns of outgoing longwave radiation that are associated with the tropical 30–60 day oscillation in Southern Hemisphere summer (NDJF) (see Fig. 8). The patterns appear in typical sequences: $\cdots \rightarrow \mathbf{q}^r \rightarrow -\mathbf{q}^i \rightarrow -\mathbf{q}^r \rightarrow \mathbf{q}^i \rightarrow \mathbf{q}^r \rightarrow \cdots$. (a) Imaginary component $\mathbf{q}^i$ (W m^{-2}), (b) real component $\mathbf{q}^r$ (W m^{-2}), and (c) explained variance (%).

characteristics of a vector time series. The basic idea is to isolate one- and two-dimensional subsystems of the full system that are controlled by linear dynamics.

We think that the POP method represents the most consistent way of doing so, but there are certainly other techniques around that can be used successfully for

similar purposes. An alternative is the *complex empirical orthogonal function* analysis (CEOF: Wallace and Dickinson 1972; Barnett and Preisendorfer 1981). CEOFs are obtained by applying the regular EOF technique to a complex time series whose real part is the real time series that has to be analyzed and whose imaginary part is the Hilbert transform of that real time series. Thus, CEOFs are related to EOFs just like CPOPs to regular POPs. The main difference between CEOFs and POPs is that CEOFs are constructed under the constraint of a maximum of explained variance and mutual orthogonality. The characteristic times, the period, and the damping time are not an immediate result of the CEOF analysis but have to be derived a posteriori from the CEOF coefficient time series. The POPs, on the other hand, are constructed to satisfy a dynamical equation, and the characteristic times are an output of the analysis; also the complex and real POP coefficients $z(t)$ (not the real and imaginary parts!) are not pairwise orthogonal. The nonorthogonality makes the mathematics less elegant, but it is not a physical drawback because, in most cases, there is no reason to assume that different geophysical processes develop statistically independent from each other. The rate of variance explained by the POPs is not optimal and has to be calculated after the POP analysis from the POP coefficients.

The POP method is not a tool that is useful in all applications. If the analyzed vector time series exhibit a strongly nonlinear behavior, the POPs may fail to identify a useful subsystem. However, if a significant portion of the variability of a nonlinear system is controlled by linear dynamics, the POP analysis may be successful in extracting principal modes of oscillation.

A FORTRAN code as well as a manual (Gallagher et al. 1991) for the regular POP analysis is available free of charge at the Deutsches Klimarechenzentrum, Bundesstraße 55, 20146 Hamburg, Germany.

Acknowledgments. This review is dedicated to Klaus Hasselmann on the occasion of his 60th birthday.

REFERENCES

Barnett, T. P., and R. Preisendorfer, 1981: Origins and levels of monthly and seasonal forecast skill for United States surface air temperature determined by canonical correlation analysis. *Mon. Wea. Rev.*, **115**, 1825–1850.

Blumenthal, B., 1991: Predictability of a coupled ocean–atmosphere model. *J. Climate*, **4**, 766–784.

Bürger, G., 1993: Complex principal oscillation patterns. *J. Climate*, **6**, 1972–1986.

Frederiksen, J. S., 1982: A unified three-dimensional theory of the onset of blocking and cyclogenesis. *J. Atmos. Sci.*, **39**, 969–982.

Gallagher, F., H. von Storch, R. Schnur, and G. Hannoschöck, 1991: The POP Manual. Tech. Report No. 1, Deutsches Klimarechenzentrum.

Hasselmann, K., 1988: PIPs and POPs: The reduction of complex dynamical systems using principal interaction and oscillation patterns. *J. Geophys. Res.*, **93**, 11 015–11 021.

Latif, M., and A. Villwock, 1989: Interannual variability in the tropical Pacific as simulated in coupled ocean-atmosphere models. *J. Mar. Sys.*, **1**, 51–60.

——, and M. Flügel, 1990: An investigation of short range climate predictability in the tropical Pacific. *J. Geophys. Res.*, **96**, 2661–2673.

——, A. Sterl, and E. Maier-Reimer, 1993: Climate variability in a coupled GCM. Part I: The tropical Pacific. *J. Climate*, **6**, 5–21.

Mikolajewicz, U., 1990: Interne Variabilität in einem stochastisch angetriebenen ozeanischen Zirkulationsmodell (in German). Examensarbeiten 10, Max-Planck-Institut für Meteorologie, 125 pp.

Penland, C., 1989: Random forcing and forecasting using principal oscillation pattern analysis. *Mon. Wea. Rev.*, **117**, 2165–2185.

——, and M. Ghil, 1993: Forecasting Northern Hemisphere 700-mb geopotential height anomalies using empirical normal modes. *Mon. Wea. Rev.*, **121**, 2355–2372.

——, and T. Magorian, 1993: Prediction of Niño 3 sea surface temperatures using linear inverse modeling. *J. Climate*, **6**, 1067–1076.

Rasmusson, E. M., and T. Carpenter, 1982: Variations in tropical SST and surface wind fields associated with the Southern Oscillation/El Niño. *Mon. Wea. Rev.*, **110**, 354–384.

Schnur, R., 1993: Baroklin instabile Wellen der Atmosphäre: Empirisch abgeleitete Moden im Vergleich zu quasi-geostrophischer Theorie (in German). Examensarbeiten 16, Max-Planck-Institut für Meteorologie, 70 pp.

——, G. Schmitz, N. Grieger, and H. von Storch, 1993: Normal Modes of the atmosphere as estimated by principal oscillation patterns and derived from quasi-geostrophic theory. *J. Atmos. Sci.*, **50**, 2386–2400.

Selten, F. M., 1995: An efficient description of the dynamics of barotropic flow. *J. Atmos. Sci.*, **52**, 915–936.

Tang, B., 1994: Periods of linear development of the ENSO cycle and POP forecast experiments. *J. Climate*, in press.

——, G. Flato, and G. Holloway, 1994: A study of Arctic sea ice and sea level pressure using POP and neural network methods. *Atmos.-Ocean*, in press.

von Storch, H., and J.-S. Xu, 1990: Principal oscillation pattern analysis of the tropical 30- to 60-day oscillation. Part I: Definition on an index and its prediction. *Climate Dyn.*, **4**, 175–190.

——, and D. Baumhefner, 1991: Principal oscillation pattern analysis of the tropical 30- to 60-days oscillation. Part II: The prediction of equatorial velocity potential and its skill. *Climate Dyn.*, **5**, 1–12.

——, and A. Smallegange, 1991: The phase of the 30- to 60-day oscillation and the genesis of tropical cyclones in the Western Pacific. Report No. 64, Max-Planck-Institut für Meteorologie, 22 pp.

——, T. Bruns, I. Fischer-Bruns, and K. Hasselmann, 1988: Principal oscillation pattern analysis of the 30- to 60-day oscillation in a general circulation model equatorial troposphere. *J. Geophys. Res.*, **93**, 11 022–11 036.

——, U. Weese, and J.-S. Xu, 1990: Simultaneous analysis of space-time variability: Principal oscillation patterns and principal interaction patterns with applications to the Southern Oscillation. *Z. Meteor.*, **40**, 99–103.

von Storch, J.-S., 1994: Interdecadal variability in a global coupled model. *Tellus*, **46A**, 419–432.

Wallace, J. M., and R. E. Dickinson, 1972: Empirical orthogonal representation of time series in the frequency domain. Part I: Theoretical considerations. *J. Appl. Meteor.*, **11**, 887–892.

Weise, R., U. Mikolajewicz, and E. Maier-Reimer, 1994: Decadal variability of the North Atlantic in an ocean general circulation model. *J. Geophys. Res.*, **99**(C6), 12 411–12 421.

Wright, P., 1985: The Southern Oscillation—An ocean–atmosphere feedback system? *Bull. Amer. Meteor. Soc.*, **66**, 398–412.

Wu, D. H., D. L. T. Anderson, and M. K. Davey, 1994: ENSO prediction experiments using a simple atmosphere-ocean model. *Tellus,* **46A,** 465–480.

Xu, J.-S., 1990: Analysis and prediction of the El Niño Southern Oscillation phenomenon using Principal Oscillation Pattern Analysis. Examensarbeiten 4, Max-Planck-Institut für Meteorologie, 95 pp.

——, 1992: On the relationship between the stratospheric QBO and the tropospheric SO. *J. Atmos. Sci.,* **49,** 725–734.

——, 1993: The joint modes of the coupled atmosphere–ocean system observed from 1967 to 1986. *J. Climate,* **6,** 816–838.

——, and H. von Storch, 1990: Predicting the state of the Southern Oscillation using principal oscillation pattern analysis. *J. Climate,* **3,** 1316–1329.

Xue, Y., M. A. Cane, S. E. Zebiak, and M. B. Blumenthal, 1994: On the prediction of ENSO: A study with a low order Markov model. *Tellus,* **46A,** 512–540.